

Univeristy of Tartu
Faculty of Science and Technology
Institute of Chemistry

Kaspars Laizans

A method for characterization of vibration testing setups

Master's Thesis (30 ECTS)

Supervisor:

Riho Vendt, PhD

Tartu, 2014

Table of Contents

	Page
List of Abbreviations	4
1 Introduction	6
2 Theoretical background	
2.1 Introduction	8
2.2 Relations between acceleration, velocity and displacement	9
2.3 Oscillations and mass-spring-damper (MSD) system	10
2.4 Free and forced vibrations, resonance	12
2.5 Classical model	13
2.6 Current developments in vibration testing uncertainty analysis	14
3 Objectives and progress during this work	
3.1 Problem statement	15
3.2 Vibration test system of Tartu Observatory	16
3.3 Analysis of calibration data provided by the manufacturer	17
3.3.1 Measurement side	17
3.3.2 Accelerometer calibration chart analysis	17
3.3.3 Data acquisition device analysis	19
3.4 Accelerometer linearity verification	24
3.4.1 Test setup	25
3.4.2 Test results	25
3.5 Vibration controller input performance verification tests	26
3.5.1 Amplitude verification test setup	27
3.5.2 Amplitude verification measurement results	28
3.5.3 Frequency verification test setup	29
3.5.4 Frequency verification measurement results	29
3.5.5 Measurement uncertainty	30
3.6 Accelerometer mounting technique influence on response spectrum	31
3.6.1 Test setup	32
3.6.2 Test results	32
3.7 Accelerometer placement influence on measurement output	33
3.7.1 Test setup	34

3.7.2	Test results	35
3.8	Frequency response spectrum corrections	36
3.9	Uncertainty budget	40
3.9.1	Accelerometer contributions	40
3.9.2	Measurement repeatability	42
3.9.3	Within laboratory reproducibility	44
3.9.4	Uncertainty budget summary	46
4	Discussion and conclusions	49
	Summary	51
	References	52
	Kokkuvõte (Summary in Estonian)	56
	Acknowledgements	i
	ANNEXES	
	Appendix A Calibration sheets	
A.1	Accelerometer calibration sheets	ii
A.2	Vibration controller calibration sheet	iv
A.3	Vibration controller input specifications	v
	Appendix B Measurement graphs	
B.1	Accelerometer linearity measurement graphs	vi
B.2	Repeatability measurement graphs	viii
B.3	Frequency validation measurement graphs	xi
	Appendix C Program code of scripts used	
C.1	Repeatability calculation and graph generation scripts	xiv

List of Abbreviations

AC	Alternating Current
ADC	Analog-to-Digital Converter
BKSV	Brüel & Kjær Sound & Vibration Measurement A/S
CMR	Common Mode Rejection
CMRR	Common Mode Rejection Ratio
CSV	Comma-Separated Value
DC	Direct Current
DMM	Digital MultiMeter
DSP	Digital Signal Processing
DUT	Device Under Test
ENOB	Effective Number of Bits
FEM	Finite Element Modeling
FFT	Fast Fourier Transform
FRS	Frequency Response Spectrum
GPS	Global Positioning System
GUM	Guide of Uncertainty expression in Measurements
IEPE	Inbuilt-Electronics PiezoElectric
LSB	Least Significant Bit
MSD	Mass Spring Damper system
PLL	Phase-Locked Loop
RMS	Root-Mean Square

SFDR Spurious-Free Dynamic Range

SINAD Signal to Noise And Distortion ratio

SNR Signal-to-Noise ratio

SQNR Signal-to-Quantization Noise Ratio

TEDS Transducer Electronic Data Sheet

THD Total Harmonic Distortion

THD+N Total Harmonic Distortion plus Noise

TNEA Total Noise Equivalent Acceleration

TO Tartu Observatory

Chapter 1

Introduction

Environmental testing of technologies and devices is essential for ensuring success of a product, be it consumer product, automotive or of scientific instrumentation kind. Testing laboratories in Tartu Observatory (TO) were established according to the development plan of TO for years 2008 - 2013 [1]. During the development and testing of the satellite it was found out that access to testing equipment necessary to pass flight acceptance tests for launch vehicle is very limited in Estonia and almost non-existent locally in Tartu parish. TO testing facilities include all the equipment necessary for Space qualification tests of small satellites and other aerospace or automotive equipment, including thermal-vacuum chamber, thermal-humidity (environmental) chamber, anechoic chamber for electromagnetic compatibility testing, and a vibration test bench. All of the equipment is of commercial kind provided by different manufacturers with years of success in their respective fields. The problem with some consumer products in general and testing equipment in particular, is that they often are not considered *measurement instruments* and as such have no need for complete uncertainty budgets. Although some calibration certificates typically are provided with the equipment, no measurement uncertainties are provided by manufacturers or retailers. It is left to end user to compile budgets and evaluate the applicability of equipment to the task at hand.

Lack of uncertainty budget and thus, lack of understanding of behaviour of the system, may lead to overtesting or undertesting. Former may lead to unneeded expensive redesign of the product, while latter - to need for frequent on-site repairs and maintenance. Testing systems are seldom used as primary measurement systems, measurements are mostly done as a secondary control of the process, hence the seeming carelessness about the possible errors. Calibration, performed in reasonable periods typically is deemed sufficient. Due to such an attitude, uncertainties of test results are often omitted (as seen by author on some test reports). Generally accepted, as it may be, this still goes against any good practice and should be avoided.

Plenty of information is available on primary and/or secondary accelerometer standard calibration methods and procedures; advanced mathematical methods are often discussed nowadays. But no publication or reference material has been found which would explain typical vibration test system and provide in-depth information about methods of compiling an uncertainty budget. This has been set as a goal for given thesis - analysis of equipment at hand and worst-case uncertainty budget compilation.

Chapter 2 provides basic terms associated with vibration testing, as well as sources of literature in form of references for further reading. Chapter 3 introduces the available set-up and provides in-depth analysis of parts involved in measurement, followed by applicable measurement result correction factors and uncertainty analysis. Conclusions are summarized in Chapter 4, where suggestions of ways to minimize uncertainties are given as well. Calibration charts, measurement result graphs and scripts used are available in appendixes.

Chapter 2

Theoretical background

2.1 Introduction

It is unfeasible (sometimes even impossible) to test each product for years in natural environment before starting to mass-produce it (as is done in medicine). Careful planning, analysis and “time compressed” testing has been found useful for overcoming this. “Time compressed” in this case means that a structure must experience all vibration cycles expected during its life-time without interruptions, all in one go. For example, all vibration cycles expected during the 20 year life-time of a train cart can be calculated statistically (average moving speed, number of rail joints, exploitation ratios all are known, excitation profiles of joints can be measured and replicated). It is relatively easy to simulate thousands of cycles of a time-stretched process within shorter timeframe than it occurs naturally, thus “speeding up” time. Years of exploitation can be shrunk to mere hours or even minutes of testing. This allows for prediction of failures and problems and taking preventive measures to ensure lifetime of uninterrupted operations.

Apart from the train example, there are more classic examples where frequency of some phenomenon couples well with a structure under investigation, which might end in destructive resonance:

- seismic waves and buildings [2];
- breaking glass due to audible resonance;
- destruction of bridges due to resonance induced by marching soldiers [3] or wind flutter [4];
- plane breaks apart due to heavily resonating parts [5]

In order to avoid such disastrous accidents in future, multiple testing disciplines have developed since fifties, including vibration analysis and testing [6]. Later, when computing power became more accessible outside specialized computing centers, mathematical modeling become main tool for initial design validation. In ideal case all three of these disciplines should be involved in any product design in following order [7] :

- vibration analysis of a preliminary design (expert reviews for most obvious flaws);

- finite element modeling of design is often implemented in modern computer-aided design (CAD) tools, such as SolidWorks®;
- vibration testing for expected environment with analysis of results;
- if necessary – rework the design to increase natural frequency in such a manner that it goes outside expected environmental vibration range.

In modern competitive market it is essential to provide cheap products in shortest time possible while maintaining quality and reliability. Often complete overhaul of an almost finished product is preferred to loss of customer trust or even lives after detection of a critical problem. Such practices are especially common in all kinds of transport provision and automation businesses (automotive, aeronautical, naval, mining and manufacturing). Lack of proper testing may lead to [7] :

- unexpected severe machine damage which results in costly repairs;
- increased power consumption due to early non-crucial fault in the machinery;
- shipment delays; accumulation of unfinished goods and/or spoilage of raw materials;
- unnecessary overmaintaining;
- poor product quality with subsequent ruining of company image and loss of customers;
- occupational hazards and casualties.

2.2 Relations between acceleration, velocity and displacement

Classic kinematic equations describe one-dimensional motion in three terms specific to movement:

displacement (\vec{x}) is distance traveled by an object in given period of time (t) with average velocity (\vec{v}):

$$\vec{x} = \vec{v}t. \quad (2.2.1)$$

It is often defined as a vector distance from some initial point via use of unity vectors. A two dimensional example in cartesian coordinate system would be:

$$\vec{x} = x\vec{i} + y\vec{j}. \quad (2.2.2)$$

Velocity (\vec{v}) is rate of change of displacement. Since velocity has a value and direction, it is inherently a vector quantity consisting of initial velocity \vec{v}_0 and changing in time t at a rate of acceleration \vec{a} :

$$\vec{v} = \vec{v}_0 + \vec{a}t, \quad (2.2.3)$$

or expressed simply as a rate of change of displacement in time:

$$\vec{v} = \frac{\vec{x}_2 - \vec{x}_1}{t_2 - t_1} = \frac{\Delta \vec{x}}{\Delta t}. \quad (2.2.4)$$

Acceleration (\vec{a}) is rate of change of displacement. Since it is derived from velocity, it is also a vector quantity:

$$\vec{a} = \frac{\Delta \vec{v}}{\Delta t} = \frac{\vec{v}_2 - \vec{v}_1}{t_2 - t_1}. \quad (2.2.5)$$

From Eq. (2.2.4), (2.2.4) and (2.2.5) it can be seen that time and distance are base quantities, while velocity and acceleration are derived from these base quantities, in such a manner that:

$$\vec{a}(t) = \frac{d\vec{v}}{dt} = \frac{d^2\vec{x}}{dt^2}. \quad (2.2.6)$$

Or reverse operation to get displacement or velocity from acceleration value, based on initial values \vec{x}_0 and \vec{v}_0 :

$$\vec{v} = \int \vec{a}dt = \vec{a}t + \vec{v}_0, \quad (2.2.7)$$

$$\vec{x} = \int (\vec{a}t + \vec{v}_0)dt = \frac{\vec{a}t^2}{2} + \vec{v}_0t + \vec{x}_0. \quad (2.2.8)$$

These equations are used when dealing with oscillating systems and accelerometers which measure acceleration. In case the oscillation waveform and durations are known, the related quantities can be derived.

2.3 Oscillations and mass-spring-damper (MSD) system

Oscillation is a basic phenomenon when dealing with vibrating systems. It is repetitive variation of some parameters around central value. In the case of mechanical vibration it is movement of a body about the equilibrium position. Ideal harmonic oscillator consists of a body with mass M suspended from a spring with the spring constant k . According to Hooke's law, when such body is displaced by the distance \vec{x} , spring exerts restoring elastic force F_e proportional to displacement:

$$F_e = -k\vec{x}. \quad (2.3.1)$$

Such system does not take into account various sources of resistance to motion (friction in spring, air drag, etc.). In order to take these various resistances into account, a combined resistive term *damping* is used. Damping is characteristic of an oscillatory system that reduces, restricts or even prevents

oscillations from happening. Damping force \vec{F}_D is directly proportional to the velocity (\vec{v}) of the mass and opposes the motion:

$$\vec{F}_D = -c\vec{v}, \quad (2.3.2)$$

where c is damping factor – a constant of proportionality of resistance over velocity. If in Eq.(2.3.2) the velocity is expressed in terms of displacement, we obtain:

$$\vec{F}_D = -c\vec{v} = -c\frac{d\vec{x}}{dt} = -c\dot{\vec{x}}. \quad (2.3.3)$$

According to Newton's second law, the total force \vec{F}_{total} is equal to mass times acceleration, where acceleration can also be expressed in terms of displacement:

$$\vec{F}_{total} = m\vec{a} = m\frac{d^2\vec{x}}{dt^2} = m\ddot{\vec{x}}. \quad (2.3.4)$$

Since total force experienced by a body is sum of all forces, we can combine Eqs. (2.3.1)(2.3.3) and (2.3.4) into:

$$\vec{F}_{total} = \vec{F}_e + \vec{F}_D = -k\vec{x} - c\dot{\vec{x}}. \quad (2.3.5)$$

That can be rearranged as :

$$\vec{F}_{total} = \vec{F}_e + \vec{F}_D, \quad (2.3.6)$$

$$m\ddot{\vec{x}} = -k\vec{x} - c\dot{\vec{x}}, \quad (2.3.7)$$

$$\ddot{\vec{x}} + \dot{\vec{x}}\frac{c}{m} + \vec{x}\frac{k}{m} = 0. \quad (2.3.8)$$

This differential equation of second order for viscous damping has solutions in the form of:

$$\vec{x} = e^{-\alpha t} A \cos(\omega_d t + \phi), \quad (2.3.9)$$

where

$$\alpha = \frac{c}{2\sqrt{mk}},$$

$$\omega_d = \sqrt{\omega_0^2 - \alpha^2},$$

$$\omega_0 = \sqrt{\frac{k}{m}}, \text{ where}$$

ω_d is the angular natural frequency of system with damper, a is decay constant, ω_0 is the angular natural frequency of system without damper, A and ϕ are amplitude and phase determined by the initial conditions of the system. A so called *structural damping model* is a modification of viscous damping more suitable for modeling internal damping within materials, where velocity term is replaced by the displacement in phase with velocity:

$$m\ddot{x} + k(1 + i\eta)\dot{x} = 0, \quad (2.3.10)$$

where i is the imaginary unit and η is the hysteretic damping factor (fraction of energy lost in each cycle of vibration). Equality of equation to 0 implies that system is unforced. In more general terms this equation can be expressed as:

$$m\ddot{x} + k(1 + i\eta)\dot{x} = f(x), \quad (2.3.11)$$

where term $f(x)$ indicates forcing function, which can be in one of many kinds with simplest examples being:

- unforced system $f(x)=0$;
- constantly applied force $f(x)=c$, where c is constant;
- constantly ramping force $f(x)=ht+c$, where h and c are constants;
- oscillating force $f(x)=a \sin(\omega t)+b \cos(\omega t)$, where a , b and ω are constants with ω being angular frequency of applied vibrations.

2.4 Free and forced vibrations, resonance

Free vibrations is a theoretical concept where oscillations do not lose energy. Once started, the system will oscillate at its natural frequency indefinitely with constant amplitude. Damping is what makes it purely theoretical, for there is no such environment without external influences (closest to this might be the outer Space) and there is no such material which would not have internal resistance. Forced vibrations, on the other hand, are very practical. These occur when the object is subjected to periodic input of force which forces it to vibrate at a particular frequency. If an object experiences forced vibrations at its natural frequency, accumulation of energy will occur due to the constructive interference, causing significant increase in the amplitude of vibration. This effect is termed resonance. Anti-resonance is the opposite effect, when forced vibration interferes destructively with an object in motion. Anti-resonances are useful for characterization of complex systems, for they can be interpreted as resonances of the system fixed at the excitation point [8].

2.5 Classical model

Classic model described in [7] incorporates only the data acquisition part of the whole vibration system as a signal path from transducer to the display and analysis. For single-axis measurement this path consists of transducer, cable, signal conditioner, low-pass filter, analog-to-digital conversion and run-time display/analysis as shown in Figure 2.5.1. While this is still mostly true for charge transducers, modern Inbuilt-Electronics Piezo-Electric (IEPE) systems have signal conditioning microelectronic circuitry built into transducer itself, thus severely reducing influence of the cable parameters on measurement results.

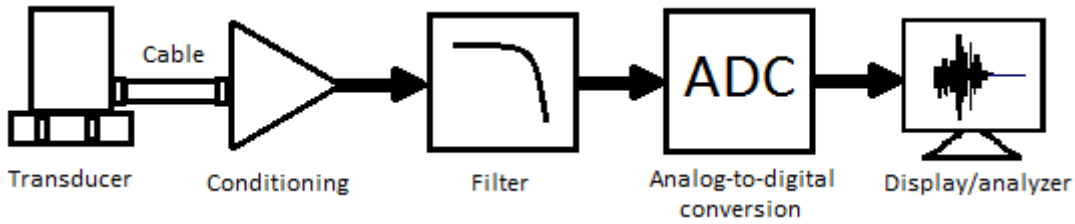


Figure 2.5.1: Signal path in classic modeling of vibration acquisition chain.

Each of these parts of data acquisition chain have their own sources of uncertainty and can be analyzed separately. Since direct transfer of mechanical motion information to a computer system is not possible, a transduction into electric signals is done according to [9], that describes direct proportional equivalence between the mass-spring-damper system and a resonant circuit consisting of passive lumped elements.

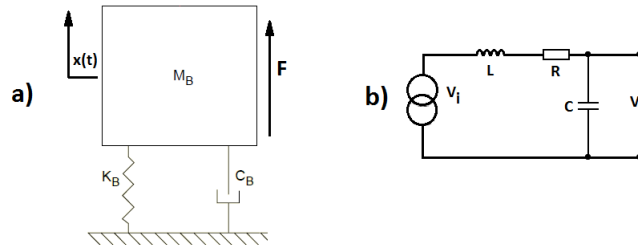


Figure 2.5.2: a) MSD and b) equivalent electric circuit (right side).

where coefficients are as indicated in Figure 2.5.2:

$q(t)$ is charge as a function of time,

L is inductance,

R is resistance,

C is capacitance and

V_i is input voltage.

Graphical representation is less obvious than comparing their characteristic equations in differential form with Eq.(2.5.1) for MSD:

$$M_B \ddot{x}(t) + C_B \dot{x}(t) + K_B x(t) = \vec{F} \quad (2.5.1)$$

and its lumped-parameter circuit system Eq.(2.5.2)

$$L\ddot{q}(t) + R\dot{q}(t) + \frac{1}{C}q(t) = V_i, \quad (2.5.2)$$

Having obtained equivalence between mechanical and electrical parameters, further analysis of data acquisition chain can be done in terms of electronic components. Figure 2.5.3 shows signal acquisition chain as a simplified equivalent electronic circuit. In IEPE devices charge amplifier is mounted in the same body as sensor itself thus minimizing influence of interface cable capacitance on high-impedance connection between sensor and charge amplifier. Charge amplifier converts this high-impedance charge into low-impedance voltage which is only minimally influenced by cable capacitance between amplifier and acquisition device. Filtering is done on the controller side along

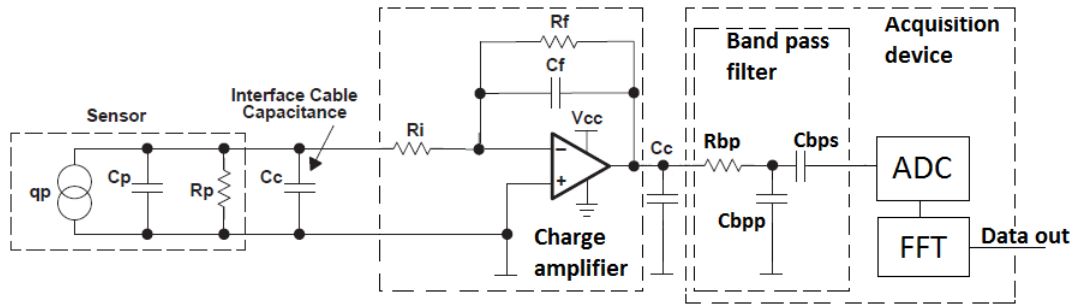


Figure 2.5.3: Signal acquisition chain modeled as electronic components.

with analog-to-digital conversion (ADC) and subsequent Fast Fourier Transformation (FFT). Output of ADC is digitized and FFT is done on the digital signal. The only thing end user (such as testing laboratory personnel) has control over is the interfacing cable between transducer and controller. Depending on manufacturer software it may be possible to adjust ADC and FFT configuration parameters as well.

Over the history of existence of vibration testing field, this has been studied extensively and nowadays is used only during the design of new systems.

2.6 Current developments in vibration testing uncertainty analysis

Recent research publications deal with more advanced problems of vibration measurements - structural dynamics [10]; multi-axial (2 and 3 D) measurements; advanced methods of random vibration characterization and synthesis of specifications [11]; statistical modeling of frequency response functions [12]; research in different models of probability [13] - Bayesian [10], fuzzy parameters; dynamic measurement error estimation [14]; analysis of stochastic processes and identification of uncertainty sources in such [15], including Monte-Carlo simulations [16, 17, 18, 19]. Large number of works dedicated to secondary-standard accelerometer calibration with either laser interferometry or in back-to-back configuration are available both in scientific journals as well as in free-form all around the Internet.

Chapter 3

Objectives and progress during this work

3.1 Problem statement

A complete vibration test bench assembly has been delivered to Tartu Observatory. Due to the proprietary nature of the vibration testing system (trade secrets, different licensing options, etc), the available data for uncertainty analysis is limited and no clearly defined procedure for measurement uncertainty estimation have been published. For complete evaluation of uncertainty it is required to know about the system as much as possible, especially when dealing with complex systems involving intermediate measurands and electronic components. A "*black box*" deduction and testing methods have to be applied to figure out inner workings of the system - an extensive knowledge about electronics and signal processing is required to complete such a task.

Accreditation of the testing laboratory to the international standard ISO 17025 requires uncertainty analysis and standardized procedures for performing tests and reporting measurement results, which were not present prior to this work.

The common approach is to state overall uncertainty level for frequency response spectrum measurement as a single percentage figure (typically "below 5 % of measured acceleration" is sufficient). Such an approach has been deemed unacceptable by author, for uncertainties related to spectral measurements tend to be frequency-dependent. An alternative method of batch-value uncertainty estimation has to be worked out.

In addition to previously stated, information on some uncertainty or imprecision sources is not available or is insufficient and have to be obtained mathematically or empirically. Uncertainty statement itself, either in "below 5% of measured acceleration" form or in tabular form is often difficult to perceive, large amounts of data best are presented in graphical form. A simple and understandable manner of depicting these uncertainties is required.

The objectives of work are as follow:

1. perform a research on uncertainty budget compilation for electro-mechanical vibration systems with generalized descriptions which should be applicable to any other accelerometer-based system with minimal modifications;

2. analysis of available specifications has to be performed first, followed by experimental derivation of missing information;
3. accelerometer output sensitivity slope deviations as well as measurement device input characteristics has to be characterized, preferably via traceable experimental setup;
4. measurement results should be corrected for dynamic changes introduced either by temperature or part of the measurement system itself;
5. devise a method of reporting measurement results graphically.

3.2 Vibration test system of Tartu Observatory

A complete vibration test bench setup was obtained for Tartu Observatory (TO) use. “Brüel & Kjær Sound & Vibration Measurement A/S” (further abbreviated as BKS SV) manufactured measurement chain is set up in combination with "LDS" exciter system. All the standard vibration test bench parts are present, their interconnection block diagram is shown in figure 3.2.1

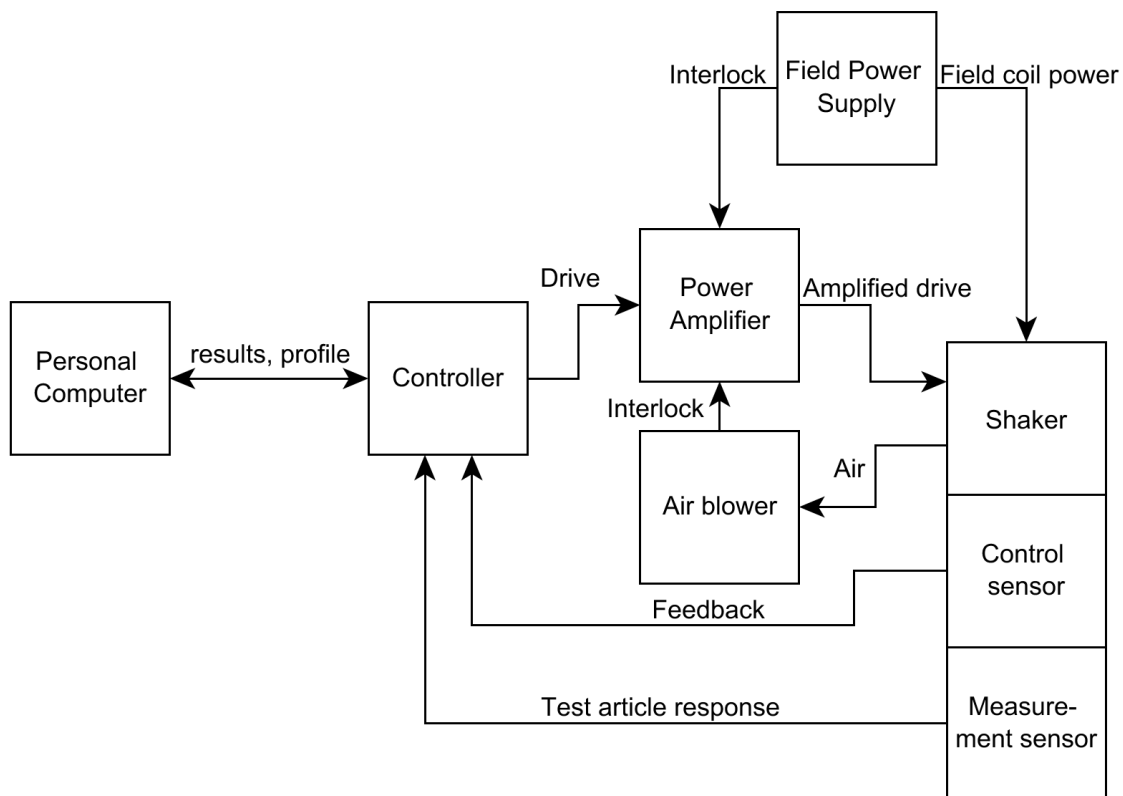


Figure 3.2.1: Vibration bench setup block diagram.

It can be noted that this is a closed-loop system, which uses feedback from the accelerometer as input of drive control algorithm.

Shaker is LDS V650 air-cooled of electrodynamic type, able to deliver up to 2.2 kN of peak force for test articles (or Devices Under Test - DUTs) with mass up to 50 kg and maximum sine peak acceleration of 980 ms^{-2} [20].

Field power supply for driving shaker field coil is FPS-10L - 70 V with up to 16 A constant drive current supply capability [21].

Power amplifier PA-1000L is 1 kW low noise adjustable-gain linear amplifier with inbuilt safety interlocks, such as overcurrent, over-voltage, open-closed loop detectors and active shaker cooling detection [22].

Cooling of the shaker is done with a suction-type air pump which provides $0.094 \text{ m}^3/\text{s}$ air flow [20].

Accelerometers, as mentioned before, are provided by BKSV, "*Type 4526-001*" 1 mV/ms^{-2} with up to 7000 ms^{-2} within 0.1 Hz to 8 kHz range [23].

Controller with both drive and measurement capabilities is also by BKSV "*Type 7541*" with 1 drive signal output and 4 inputs. It is a standalone device controlled over the computer network by a computer with BKSV software installed [24].

Software is manufacturer provided proprietary personal computer program, which interfaces with the controller hardware over the network. It requires separate licenses for different tests performed [24].

3.3 Analysis of calibration data provided by the manufacturer

3.3.1 Measurement side

Measurement side consists of three elements:

- IEPE pick-up accelerometer;
- cabling;
- data acquisition device with inbuilt analysis capabilities.

Since analysis of measurement results are supposed to be performed for Device Under Test (DUT), not accelerometer itself, two more factors should be kept in mind - accelerometer mounting technique and placement. Former strongly influences responses due to damping in coupling, while latter may change Q-factors exhibited at different mount points due to vibration modes.

3.3.2 Accelerometer calibration chart analysis

In this chapter a calibration chart [23] provided by "Brüel & Kjær Sound & Vibration Measurement A/S" (see Appendix A.1) is analyzed in detail for deeper understanding of implications these data provided may have.

Sensing element indicates the material used in production of sensor itself. PZ23 is artificially polarized lead zirconate titanate with approximate sensitivity of 300 pC/N . Coupled with weight of seismic mass, this information is used as a basis for final transducer sensitivity calculations.

Reference sensitivity at a specific frequency (159.2 Hz) measured with certain input parameters (20 ms⁻² Root-Mean-Square (RMS) input with 4 mA supply current) at specified temperature.

Frequency range is linear measurement range within which measured self-response deviates from reference by <10 % for amplitude measurements and <5 % for phase response. Typically upper 10 % limitation is set as 0.30 of resonance frequency.

Mounted resonance frequency is a natural response frequency of accelerometer when it is mounted as stiffly to the exciter as possible (typically stud-mounted), when influence of errors due to mounting can be neglected.

Transverse sensitivity is accelerometer's sensitivity to vibrations orthogonal to the main sensitivity axis. In ideal case it should be 0, but in practice there are some values present due to manufacturing tolerances. Values are indicated as percentage of main axis sensitivity at some arbitrarily selected frequency.

Calculated values for TEDS are values which are stored in the accelerometer's internal memory for later acquisition by a capable system via 1Wire communications according to [25]. These include:

- Resonance frequency;
- Quality factor at resonance;
- Amplitude slope is term used to describe change in sensitivity within the linear range. Unit *decade* denotes a factor of 10 difference between two numbers. E.g. following sequence has one decade difference between each: 10-100-1 000-10 000;
- High-pass cut-off frequency is the lowest frequency accelerometer is able to measure due to inbuilt electronics. These limitations are set by time constant associated with feedback circuit on charge amplifier. Piezoelectric accelerometers are self-generating devices which produce output as a response to dynamic force, static force lacks dynamic component and would not provide any output, therefore it is impossible to get a true DC response.
- Low-pass cut-off frequency is a result of an additional filter set up specifically to remove high-frequency noise which can have appreciably higher levels than vibrations within the band of interest. If these frequencies are not filtered out, they might overload the inbuilt amplifier and create overall clipping effects which would incorrectly appear as a low level of response.

Bias voltage is a level of DC voltage which is taken as a *virtual ground* level for AC signal. In DC systems it is undesirable for potential to go below ground level (0 V), so an offset or bias voltage is set about which AC is fluctuating. Does not have influence on uncertainty estimation as long as measurement is performed within normal range (no amplitude clipping);

Inherent noise determines the lower resolution limit of the sensor which arises purely within built-in electronics of accelerometer due to thermal electron movement. This parameter has multiple sub-parts:

- broadband RMS value over the whole linear range;
- spectral noise density measured at specific frequencies (usually decade apart).

Equivalent noise acceleration a_x (also known as *Total Noise Equivalent Acceleration - TNEA*) is indicated as noise voltage u_x and transducer sensitivity B_{ua} ratio [26]:

$$a_x = \sqrt{\frac{4k_b T \omega_x}{Qm}} = \sqrt{\frac{u_x}{B_{ua}}}. \quad (3.3.1)$$

Classic kinetics (first part of Eq.(3.3.1)) explain this noise in thermal terms - Boltzmann's constant k_b , absolute temperature T , frequency ω_x , mass m and quality factor Q .

Since individual spectral noise levels are indicated in RMS terms, it is possible to interpolate noise level a_x for intermediate frequency f_x by taking square root of difference between closest two frequencies f_1 and f_2 with respective stated noise levels a_1 , a_2 and multiplying it by noise density stated for lower limit, as recommended by [27]:

$$a_x(f_1 < f_x < f_2) = \sqrt{a_{f_2} - a_{f_1}} \cdot a_{f_1}. \quad (3.3.2)$$

[28] indicates that for low frequencies (below 100 Hz) generally it can be approximated as a *pink noise* with inverse-frequency dependence:

$$a_x = \frac{1}{f_x}. \quad (3.3.3)$$

Temperature coefficient of sensitivity indicates sensitivity to thermal drifts as a full-scale sensitivity percentage per °K (°C given in certificate) from calibration temperature.

Magnetic sensitivity is reading distortion due to strong environmental magnetic fields.

Mechanical and electrical parameters, such as mass, impedance and power supply requirements do influence generation of response characteristics.

3.3.3 Data acquisition device analysis

“Type 7541” vibration controller by “Brüel & Kjær Sound & Vibration Measurement A/S” [24] also came factory calibrated. Calibration of only output and four input channels was stated for voltage offset and gain errors. Output was calibrated for 0.1 V and 10.0 V ranges, while inputs for 0.2 V and 20.0 V. Final stated errors for this instrument are shown in Table 3.3.1. These errors should

Table 3.3.1: Stated errors for the vibration controller

Channel ID	Offset / V	Gain Error / %
Output 1	0.00001	0.0
Input 1	0.00018	0.0
Input 2	0.00028	0.0
Input 3	0.00033	0.0
Input 4	0.00010	0.0

be included into final correction factor, but they do not provide much information about sources of uncertainty.

Uncertainty sources can be obtained from vibration controller specification analysis once complete understanding about its principles of operation is available. An excerpt of specification is available in Table 3.3.2. Since scope of this paper is measurement data acquisition side, only values for inputs are indicated.

Table 3.3.2: Excerpt from Type 7541 vibration controller specification [24]

Specification	Value declared
Frequency Range	DC to 46 kHz with 54 cutoff frequencies
A/D Conversion	2 x 24 bit
Data Transfer	24 bit
Input Voltage Range	$\pm 20 V_{peak}$
Spurious-free Dynamic Range	130 dB typical
Harmonic Distortion (all harmonics) Plus Noise	-100 dBfs (DC to 1 kHz) typical
Crosstalk: Between any two channels of a module	< -100 dB typical
Common Mode Rejection in 10V _{peak} input range	> 90dB typical
Absolute Amplitude Precision, 1 kHz, 1 V input	0.5% FS

Vibration controller's acquisition part or *input* consists of two main components - analog-to-digital converter (ADC) and Digital Signal Processing (DSP) unit. Since DSP deals with purely digitized data, it is assumed that it does not introduce any errors apart from rounding error of *floating point* numbers. Assuming, that DSP used is 32 bit one, where 23 bits are used for actual number storage, rounding error according to [29] with most conservative approach can be up to ± 0.5 LSB (least significant bit) value, where LSB is calculated as:

$$LSB = \frac{V_{FS}}{2^B}, \quad (3.3.4)$$

where V_{FS} is full scale (difference between maximum and minimum measurable values) voltage and B is number of used bits in the system.

Entering specified values into Eq. (3.3.4), we obtain theoretical LSB value for full-swunged measurement:

$$LSB = \frac{20 \text{ V} \cdot 2}{2^{24}} = \frac{40 \text{ V}}{16777216} = 2.4 \mu\text{V}. \quad (3.3.5)$$

Unlike DSP, which is difficult to analyze with "black-box" approach due its programmatic nature, ADC is widely used and understood procedure. Errors introduced by ADC are more numerous and complex than those of DSP. Ones given in specifications are:

Input voltage range is maximum measurable input voltage given in $\pm V_{peak}$ form. To obtain *peak-to-peak* or *full scale* (V_{FS}) value, this should be multiplied by two. This is used as a basis for other ADC parameter calculations.

Analog to digital (A/D) conversion is term describing quantization step. Given as "2 x 24 bit" it might be confusing, but data bus width stated in **data transfer** section indicates that only one channel is used at a time (since data bus width is only 24 bits), which leads to assumption that each of ADC channels measure their own polarity of the wave - one measures positive side, while other - negative. This gives full scale quantization step as:

$$Q(x) = \frac{V_{FS}}{2^B}. \quad (3.3.6)$$

It may be noted, that quantization step $Q(x)$ formula is the same as LSB calculation formula in Eq.3.3.4, which is true, for in this case least significant bit value is actually obtained from ADC. The actual LSB value may differ from value output from ADC due to possible signal conditioning performed on full-scale input voltage V_{FS} . Values in equation (3.3.5) should be corrected to take into account assumed use of two ADCs, each for one polarity of waveform:

$$Q(x) = LSB = \frac{20\text{ V}}{2^{24}} = \frac{20\text{ V}}{16777216} = 1.19\mu\text{V}, \quad (3.3.7)$$

which would result in DSP rounding error of:

$$\sigma_{DSP} = 1 \cdot LSB = 1.19\mu\text{V}. \quad (3.3.8)$$

Quantization procedure in ideal ADC would have an uniformly distributed rounding error within range of ± 0.5 LSB. Quantization error is uniformly distributed between two adjacent values with rectangular probability of accuracy of both - rounding up or down:

$$\sigma(Q)_{DSP} = \frac{Q(x)}{\sqrt{12}} = \frac{1.19\mu\text{V}}{\sqrt{12}} = 0.34\mu\text{V}. \quad (3.3.9)$$

An aggregate of all quantization products that are not desired signal is a *residual error* which is quantified as a *bits lost* (B_l) term [30]. This accounts for such parameters as nonlinear distortion, quantization error and random noise. This is a ratio of quantization steps of an ideal ADC and a real ADC, which has its *effective quantization interval* $Q(x)_{eff}$:

$$b_l = \log_2 \left(\frac{Q(x)}{Q(x)_{eff}} \right). \quad (3.3.10)$$

Spurious-Free Dynamic Range (SFDR) is defined as a ratio of RMS full-scale signal amplitude A_{FSRMS} to the RMS value of peak spurious spectral component $A_{spurRMS}$ [31]:

$$SFDR = 20 \cdot \log \left(\frac{A_{FSRMS}}{A_{spurRMS}} \right) \text{ dB}. \quad (3.3.11)$$

Normally SFDR is given for whole usable bandwidth (limited by Nyquist frequency $\frac{f_n}{2}$), which in our case is stated from DC to 48 kHz. SFDR is more sensitive measurement than typical signal-to-noise ratio measurement, for FFT gain (33 dB for 4096-point FFT) reveals these peaks [31]. The significance of this parameter is that it indicates how well ADC detects changes in small amplitude signals in presence of large amplitude noise, which can mask or degrade the actual signal. As [30] notes, that ideal ADC yield SFDR maximum values at full scale input, while real devices exhibit best SFDR way below full scale (at least several dB). This is an indicative parameter and should not impact measurement uncertainty, for it is already included into THD+N component (see following paragraph).

Total Harmonic Distortion plus Noise (THD+N) assesses the energy content of harmonics of original signal with all other noise components included (except Direct Current (DC)). In special cases when full bandwidth up to Nyquist frequency is used, THD+N is equal to Signal-to-Noise-And-Distortion ratio - SINAD. Since measured range is specified (up to 1 kHz), this approximation is not exactly valid, for THD+N in this case has to include whole measurement range.

Signal-to-noise ratio is a comparison of desired signal level to the system noise. [32] offers approximation of maximum Signal-to-Quantization Noise Ratio (SQNR) for sine wave acquired with B bit resolution as

$$SQNR \approx 1.761 + 6.02 \cdot B \text{ dB}, \quad (3.3.12)$$

so, for an ideal 24 bit ADC system we obtain SQNR as:

$$SQNR_{24bit} = 1.761 \text{ dB} + 6.02 \text{ dB} \cdot 24 = 146.241 \text{ dB}. \quad (3.3.13)$$

[31] defines SINAD as a function of SNR and THD

$$SINAD = -10 \log \left(10^{-SNR/10} + 10^{-THD/10} \right). \quad (3.3.14)$$

Inserting values from Table 3.3.2 and Eq. (3.3.13) into previous formula, we obtain numerical SINAD value:

$$SINAD = -10 \log \left(10^{-146.241/10} + 10^{-100/10} \right) = 99.99 \text{ dB}. \quad (3.3.15)$$

Effective Number Of Bits (ENOB) of a real ADC is computed by inverting SQNR equation (3.3.13) to obtain number of bits using calculated SINAD as SNR value:

$$ENOB = \frac{SINAD - 1.76}{6.02} = 16.61 \text{ bit}. \quad (3.3.16)$$

ENOB is a figure of merit which allows to calculate effective quantization step $Q(x)_{eff}$ which takes noise into account and produces equivalent to ideal ADC device without noise. Although expressed in terms of ideal ADC, this is *real* device parameter. For given vibration controller, effective quantization step after taking all noise sources into account would be:

$$Q(x)_{eff} = \frac{V_{FS}}{2^{ENOB}} = \frac{20V}{2^{16.61}} = 199.77 \mu V. \quad (3.3.17)$$

Quantization error has to be re-estimated to take into account this effective quantization step:

$$\sigma(Q(x)_{eff}) = \frac{Q(x)_{eff}}{\sqrt{12}} = \frac{199.77 \mu V}{\sqrt{12}} = 57.67 \mu V. \quad (3.3.18)$$

Crosstalk between any two channels is an estimate of electronic interference originating from common supplies or electro-magnetic induction and similar effects. Stated as <-100 dB should be applied separately in the presence of another signal. -100 dB in linear scale would be coefficient of 0.00001 times input voltage on adjacent channel.

Common mode rejection (CMR) is ability of the device to reject unwanted signals present on both input leads. These unwanted signals might arise from component mismatches and tolerances, or other low-level component errors. CMRR (common mode rejection ratio) is CMR expressed as a ratio of rejection relative to required signal difference. Offset error due to CMRR is defined as [33]:

$$\sigma_{CMRR} = \frac{V_{in}}{CMRR}. \quad (3.3.19)$$

To obtain numerical value, stated 90 dB CMR has to be converted to linear CMRR and input into Eq. (3.3.19):

$$\sigma_{CMRR} = \frac{10V}{1000000000} = 0.06 \mu V. \quad (3.3.20)$$

Total uncertainty of digitized spectra amplitude would yield:

$$\begin{aligned} u(Input) &= \sqrt{\sigma_{CMRR}^2 + \sigma(Q(x)_{eff})^2 + \sigma(Q)_{DSP}^2} = \\ &= \sqrt{(0.06 \mu V)^2 + (57.6687 \mu V)^2 + (0.3441 \mu V)^2} = 57.67 \mu V. \end{aligned} \quad (3.3.21)$$

Relative full-scale input uncertainty would be

$$u(Input)_{rel} = \frac{u(Input)}{V_{FS}} \approx 0.003 \%. \quad (3.3.22)$$

Absolute amplitude precision is a measure of offset and shall be included into measurement correction factor as calibrated bias.

3.4 Accelerometer linearity verification

Two calibrated accelerometers are available with specified sensitivity changes over the frequency range. Manufacturer provides information on these changes as graphs and as an amplitude sensitivity change slope. However, it can be seen in Figure 3.4.1 that there are minor sensitivity peaks in graphs (see Appendix A.1 for separate original calibration charts) which cannot be extracted from linear slope, but could be useful for increased measurement precision. Graphical analysis of graphs was performed. Sensitivity mismatches at the beginning of the graph (up to 15 Hz) and end of the graph (after 3 kHz) as well as peaks and bumps at 50 Hz and 600 Hz are clearly visible. Less visible is waviness of graphs in opposite phases at 200 Hz, which were lost during the image extraction. From 2% to 5% variations in sensitivity are present, even taking into account stated slope some parts of spectrum still vary by a per cent or two. At a full-scale range of 7000 ms^{-2} , this would mean an error of up to 69 ms^{-2} to 137 ms^{-2} . A method should be devised for obtaining numerical values from transducers themselves with an existing system. Having an open loop system would be beneficial for

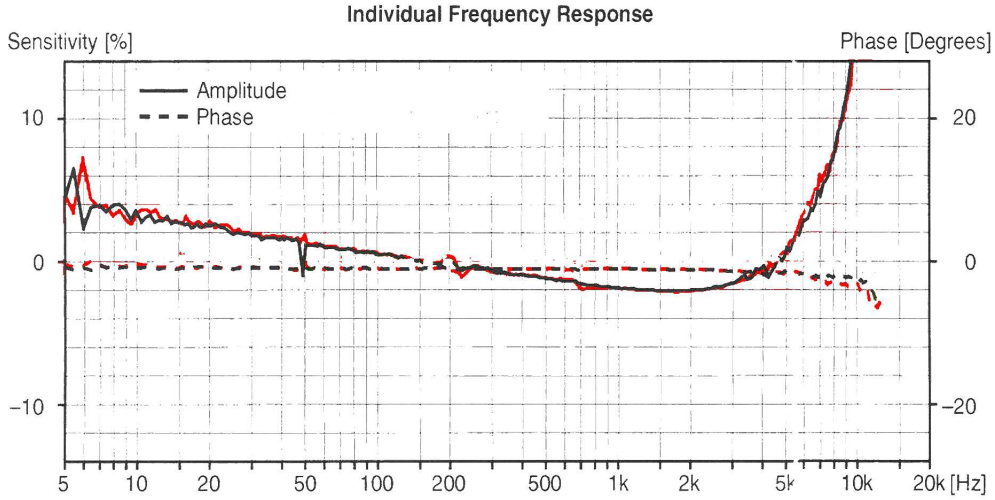


Figure 3.4.1: Comparison of two accelerometer sensitivity changes [23] (see Appendix A.1 for separate graphs). Black is accelerometer 1, red is superimposed graph of accelerometer 2.

this purpose, for both accelerometers would just output their real responses to a constant excitation level. A closed loop system increases the final calculation complexity, if it is unable to work in open-loop mode. In this case it is question of separating sensitivity changes of measurement and feedback accelerometers.

According to individual frequency response calibration graphs, deviation of measured frequency response $C_{sens}(f)$ from reference sensitivity should be visible and calculable as a response amplitude $A_{response}$ fraction of drive amplitude A_{drive} difference from reference sensitivity S_{ref} :

$$C_{sens}(f) = \left(\frac{A_{response}}{A_{drive}} \cdot S_{ref} - S_{ref} \right) \cdot 100\%. \quad (3.4.1)$$

So change in frequency response $C_{sens}(f)$ can be calculated if stable (and preferably with constant level) drive signal is provided and reference sensitivity is known.

Closed loop system which uses one accelerometer as feedback for drive level adjustment incorporates this change in accelerometer sensitivity into its drive algorithm - drive level will be offset by accelerometer sensitivity change value in such a manner, that constant level will be measured. This change should be taken into account when developing vibration profiles to ensure that correct accelerations are applied to the test article. The problem with existing system is that amplifier was found out to be non-linear, meaning that constant input voltage will generate output varying in a non-linear manner when viewed either in time or frequency domain. Such non-linearity forbids to measure actual absolute accelerometer sensitivity changes over frequency, but a method was devised to measure differences between outputs of accelerometers. Having obtained these differences (A_{peaks}), they can be added with linearity slope $\frac{dA}{df}$ stated in calibration certificate to obtain final sensitivity change correction graphs which have to be applied to measured response $A_{measured}$:

$$C_{sen}(f) = A_{measured} + \frac{dA}{df} + A_{peaks}. \quad (3.4.2)$$

When controller uses one accelerometer as feedback, it incorporates deviations from perfect linearity into drive signal - temporary increase in sensitivity will force drive level to be reduced temporarily. Second accelerometer would measure all the peaks emanating from both accelerometer sensitivity changes, direction of the offset would indicate opposite of sensitivity change. Separation of measurement accelerometer peaks from feedback accelerometer peaks should be possible using small peaks in drive signal when it is compensating for variations in feedback sensitivity.

3.4.1 Test setup

Two accelerometers were mounted on a dummy mass (interface fixture) as closely as possible to each other with stud mounts. Constant acceleration was applied in both - open and closed loop configurations, while measuring output generated by the accelerometers. Measurements were done as a full-band sweep from 5 Hz to 4000 Hz as well as localized around expected deviation regions of 50 ± 20 Hz, 200 ± 40 Hz and 700 ± 100 Hz.

3.4.2 Test results

Results obtained during these tests are inconclusive. On graphs with unaltered measured both channel accelerations (see Appendix B.1) there do appear patterns similar to the ones indicated in calibration charts, but they are offset from stated frequencies and are of amplitude values inconsistent with those expected. The differences between measured response amplitudes are due to linear part of sensitivity differences as well as transmissibility of mounting surface. Proposed method does not work well with offsets of such small amplitude percentage - they get drowned in system noise (2% of 1 mV/ms^2 is approximately $20 \text{ } \mu\text{V}$, which is below $57 \text{ } \mu\text{V}$ quantization noise of the system). A known and stable external reference should be used for measurements with high resolution requirements, as well as digitization device with lower inherent noise. Manufacturer's stated linear change in sensitivity is going to be used as a correction factor without taking into account missing peaks. Zones of extended

uncertainty can be established around frequencies with peaks, equal to approximation of peak-to-slope difference shown in Table (3.4.1).

Table 3.4.1: Additional uncertainty values for zones with sensitivity peaks.

Center frequency / Hz	Bandwidth / Hz	Increase in uncertainty / % S_{ref}
6	1	4
10	6	2
47	10	2
200	80	1
700	100	0.5

This approach may lead to overestimation of the uncertainty, but it is acceptable, for aim of this work is to compile most conservative uncertainty budget.

3.5 Vibration controller input performance verification tests

Vibration controller input is ADC based digitization device, hence it may have discrepancies in quantization steps, both in time-base and in amplitude. Typical modern ADC devices are capable of measuring high frequency signals, within orders of magnitude of range required for vibration testing should not be a problem. There may, however, be some specific offsets from manufacturer-stated linearity due to manufacturing tolerances. This test is intended to measure amplitude and frequency measurement accuracy of the input.

Since accelerometers are of IEPE type, the cable from accelerometer to controller input not only carries AC signal of response, but also DC current required to power the built-in electronics. This DC current source I_{const} is incorporated into controller in such a manner, that signal electrical path shown in Figure 2.5.3 on acquisition side becomes as shown in Figure 3.5.1. DC current injected is blocked out by built-in band-pass filters, so it is not measured by the ADC.

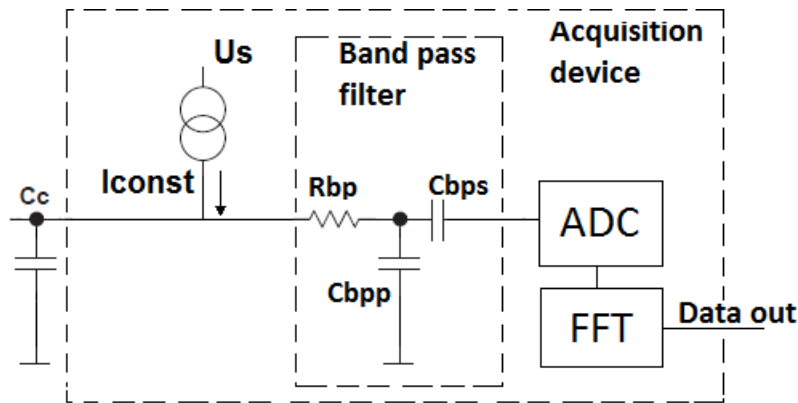


Figure 3.5.1: Signal electrical path on acquisition side with incorporated constant current source.

Since the goal of this test is to evaluate frequency and amplitude measurement errors of acquisition device, an external reference should be used, which is able to generate stable both in time and amplitude sine wave which can be measured by the controller. Whole system should be able to operate in some *simulation mode* without shaker or accelerometers.

3.5.1 Amplitude verification test setup

Vibration controller input is connected to the sine-wave generator, while output is left floating. Sine-wave generator uses external traceable frequency reference for feeding Phase-Locked Loop (PLL), which outputs stable sine-wave of required frequency phase-locked with reference. Phase-locking of low generated frequency to high reference frequency is very effective from the point of view of errors, especially if difference is measured in integer multiples. Functional block diagram is shown in Figure 3.5.2.

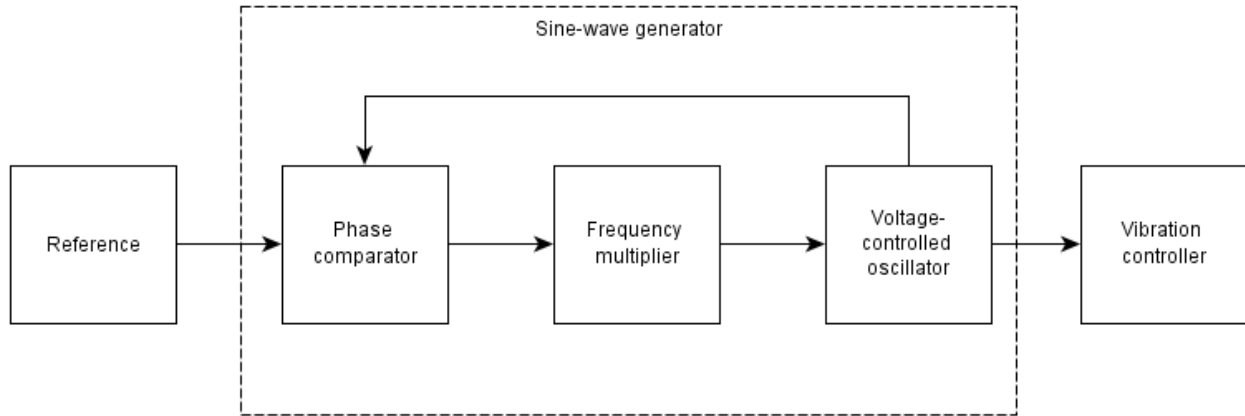


Figure 3.5.2: Sine reference signal feed functional block diagram.

Frequency reference available in Tartu Observatory is "Pendulum GPS-89" by SpectraCom Inc [34]. It is GPS-controlled precision frequency source with inbuilt Rubidium standard as a back-up. It has 10 MHz output traceable to Swedish National Testing and Research Institute with 10^{-12} Hz frequency stability [35].

Sine generator is BKS *Type 1049* [36] with frequency range from 0.2 Hz to 200 kHz and output amplitude range from 100 μ V to 5 V. Since external reference is used, internal clock stability is not an issue, for it is not used.

DC blocking capacitor has to be installed in series between generator and vibration controller to prevent damage to sine generator output, which could result from current injection done by controller. Parameters of this capacitor can be derived from the controller specifications:

- Voltage rating depends on largest of both - AC or DC component. A generated sine-wave with 1 V RMS value is planned to inject into system, while accelerometer power supply is stated in range of up to 30 V. Standard ratings next to this value are 25 V and 50 V. Latter is preferred for safety reasons;
- Capacitance depends on the lowest frequency capacitor should be able to let through, as well as input impedance of the load. Load in this case is controller's input impedance, which is stated as 500 k Ω in single-ended mode and 1 M Ω in differential mode. Publication [37] recommends

selecting roll-off frequency (frequency at which signal starts to attenuate) at 1/10th of a frequency of interest, for first order filters have roll-off value of around -20 dB/decade. With range of interest being from 5 Hz to 4000 Hz and additional margin of error of 2 Hz (typical Z-class capacitors tend to have tolerances up to -20% to +80%) 3 Hz was taken as a baseline for calculations, which leaves with desired -3 dB cut-off frequency f_c of $0.1 \cdot 3 \text{ Hz} = 0.3 \text{ Hz}$. Capacitor impedance (X_C) formula can be used with these data to calculate capacitance value C needed for proper blocking of DC while allowing AC with frequency of interest to pass through:

$$X_C = \frac{1}{2\pi f_c C}. \quad (3.5.1)$$

Rearranging Eq. (3.5.1) to solve for C and inserting values, we can obtain capacitance required:

$$C = \frac{1}{2\pi f X} = \frac{1}{2\pi \cdot 0.3 \cdot 500000} = 1.061 \cdot 10^{-6} \text{ F}. \quad (3.5.2)$$

Taking closest standard value of 1 μF will yield change in frequency insignificant, compared to standard tolerances.

Test is expected to be run as a constant-amplitude sweep of 1 V peak over usable frequency range of 5 Hz to 4000 Hz.

Agilent U1242B [38] digital true-RMS multimeter was added in parallel to the vibration controller to verify the signal amplitude measurements.

3.5.2 Amplitude verification measurement results

Amplitude averaging was done using the peaks measured during the frequency verification test. It was found out that synchronizing the start of the signal generation and acquisition systems is problematic. Lack of such synchronization leads to measuring side of the waveform, not the crest. During standard sweeping measurement difference of the measurement point to crest changes with frequency (due to varying generator bandwidth) which may lead to erroneous conclusions. Peak-detection method was deemed to be more accurate. Amplitude values of detected peaks are averaged and compared to the average amplitude measured with DMM, which in Table 3.5.1 are denominated as *Reference value*. This allows to evaluate input offset errors and compare them to ones stated in calibration chart. These offsets then can be incorporated into measurement result corrections. Results are summarized in Table 3.5.1:

Table 3.5.1: Voltage amplitude verification measurement results.

Frequency / Hz	Measured value / mV	Reference value / mV	Offset / mV	Uncertainty / mV ($k=2$)
10	999.2	965.6	33.60	75.20
100	1002	1001.0	14.32	75.20
1000	1001	1002.1	-0.74	75.20
3950	1001	1002.0	-0.92	75.20

Largest source of uncertainties are DMM and signal generator. Generator has unstable peak value at frequencies below 1000 Hz, which contributes greatly on the statistical error, although it is still way below stated calibration aging value of the multimeter.

3.5.3 Frequency verification test setup

Verification of input frequency measurement accuracy was performed using the same equipment and setup as in amplitude verification test. Main difference between these tests is procedure used. Amplitude measurement over the whole range of interest is expected to be constant, hence it can be swept multiple times and averaged. Frequency verification measurement requires knowledge of the location of each individual peak in frequency domain. Even taking into account only integer values of frequencies, measuring 4000 individual frequencies at least 5 times (to satisfy minimum number of measurements for statistical analysis) would be too time-consuming to be reasonable. The measurement time increases exponentially with increase of desired resolution, so some sort of a trade-off has to be chosen.

Measurement method involves generating a wave with constant frequency and amplitude and measuring it on the controller. Since no real generator is perfect, sidebands are expected to appear on measurement results, as well as some broadening of the spectrum measured - it will not be straight line but in the form of sinc function graph. Additional broadening will be introduced by the sampling bandwidth of the measurement system which has minimum bandwidth value of 1.01 Hz. Table 3.5.2 summarizes planned test parameters of this measurement.

Table 3.5.2: Frequency sweep parameters for frequency verification tests.

Center frequency / Hz	Sweep bandwidth / Hz	Sweep speed / Hz/s	Resolution / mHz
10	4	0.1	2.44
100	8	0.1	2.44
1000	10	0.5	10.26
3950	20	0.5	24.4

Measurement is done by sweeping over the generated center frequency and logging amplitude. Central frequency measured is assumed to be the one with highest amplitude peak which should be a unique value (off-center values are expected to be at least duplicated with one copy on each side of the main lobe). Sweeps are done in “up” and “down” directions (increasing frequency and decreasing it) to evaluate influence of the delays due to calculations, each at least 5 times.

3.5.4 Frequency verification measurement results

Frequency verification measurement results (see Appendix B.3 for graphs) indicate, that there is an offset from desired response. This offset is sweep-direction dependent - sweeping in “up” direction results in mostly in positive or near-zero values if negative, while opposite sweep direction results in negative offset. Frequency measured with DMM was taken as a reference value for which uncertainty was calculated according to [39].

Table 3.5.3: Frequency verification measurement results.

Center frequency / Hz	Offset “up” direction /mHz	Expanded uncertainty ($k=2$) / mHz	Offset “down” direction / mHz	Expanded uncertainty / mHz ($k=2$)
10	81.8	131.5	- 83.3	131.5
100	23.7	795.2	- 21.7	795.2
1000	-3.1	7959.1	- 9.2	7959.1
3950	75.7	7755.1	- 26.9	7755.1

From the results shown in Table 3.5.3 it seems that offset values vary randomly, so for uncertainty analysis it will be assumed a random variable and average of all the measurements will be taken. For high-reliability measurements it is recommended to do sweeps in both directions with averaging of both presented as a final measurement. This will significantly increase the final frequency uncertainty values but will provide more trustworthy results. Maximum frequency uncertainty obtained during these measurements is 0.78% over the large part of range of interest.

3.5.5 Measurement uncertainty

Since measurands in this test include both - frequency and amplitude, both uncertainties should be included into results. Initially an attempt was made to quantify uncertainties originating from the signal generation chain. This approach yielded unsatisfactory results, despite the complexity of the parameters involved - combined uncertainty was in par of that acquired with a simple multimeter. A simpler approach was chosen, where digital multimeter was used for output amplitude and frequency verification. Only uncertainties associated with this measurement device will be taken into account. Such an approach dramatically simplifies calculations and increases reliability of the measurement, for each part of generator chain contains multiple ambiguous parameters, misinterpretation of which may lead to erroneous assumptions. As for frequency measurement uncertainties - they mainly arise from the reference clock generator multiplied by PLL conversion factor and generator resolution, which could still yield higher result resolution but again with unknown error margins.

Calculations with uncertainties associated with DMM have been done in accordance with [39] guidelines. Measurement points were chosen such, which would provide highest precision as close to the frequency of interest, as possible. For example, 99.99 Hz and 999.99 Hz are sensitivity change points for DMM, meaning that measurements at 100 Hz or 1 kHz would provide much more uncertain result, than those obtained at slightly lower frequency. Frequency generator linearity allows such shift with negligible level of error.

Effective number of degrees of freedom for each measurement are calculated using Welch-Satterthwaite formula given in Eq. (3.5.3)

$$v_{eff} = \frac{u_c^4(y)}{\sum_{k=1}^N \left(\frac{c_k^4 u_k^4(x_k)}{v_k} \right)} \quad (3.5.3)$$

Table 3.5.4: Reference voltage and frequency measurement results

Center frequency	Measurand	Average	Mean standard deviation	Resolution	Standard Uncertainty	DoF
10.0 Hz	Frequency	9.993 Hz	0.1 mHz	10 mHz	56.7 mHz	2240
10.0 Hz	Voltage	965.6 mV	570.5 μ V	1 mV	36.6 mV	1632
99.0 Hz	Frequency	98.998 Hz	0.1 mHz	10 mHz	397.6 mHz	957
99.0 Hz	Voltage	1.001 V	0.0 μ V	1 mV	36.6 mV	979
995.0 Hz	Frequency	994.999 Hz	0.2 mHz	100 mHz	3.99 Hz	1959
995.0 Hz	Voltage	1.001 V	9.7 μ V	1 mV	37.2 mV	713

Generally large numbers of measurements (over 100) have been done with comparatively small standard deviations of the mean, which results in coverage factor $k=2$.

Uncertainty of measured amplitude has to include reference uncertainty (arising from DMM) as well as statistical and digitization errors.

3.6 Accelerometer mounting technique influence on response spectrum

There are many accelerometer mounting techniques used in vibration testing:

- stud mounting with a steel stud is most preferred and recommended to use whenever possible. This method ensures the best coupling between DUT and accelerometer and allows achieving highest mounted resonance frequency, especially if coupling surface is filled with silicone grease or other filling agent for gap reduction [40];
- cementing a stud with epoxy or cyanoacrylates (hard instant glues) is next preferred option when drilling a hole for stud mounting is considered unfeasible. Dental cements also seem to be quite popular for given application. Frequency responses are reported to be nearly as good as with plain stud mounting. Cementing accelerometer itself to DUT is not recommended, for difficulties may be encountered in removing it after the test – corrosion damage in case of chemical removal of adhesive or shock damage if sensor is just snapped off;
- mounting with a permanent magnet is much appreciated in modal testing of ferromagnetic devices, due to ease of attachment or just quick moving over flat surfaces for large numbers of repeated tests at different measurement points. Dynamic range is slightly limited due to limited force of the magnet, but frequency response is adequate, especially at high frequencies;
- mounting clips are also a feasible solution for tests which have to be repeated at irregular intervals. Clips themselves can be mounted rigidly by using stud mount or cementing, while accelerometer can be snapped in place whenever needed. Care has to be taken to detect wear of clips;
- double-sided adhesive tape is used often in non-destructive testing of unique equipment which should not be damaged or modified in any way. It is easy to install, easy to remove and difficult

to estimate effects of different tapes on the results obtained. Variance of elasticity of tape and adhesive as well as thickness of both is too high to be predictable and non-reusability of singular patch makes it impossible to cross-compare with a reference;

- special swivel bases are available for aligning axes of motion with axis of sensitivity. Care must be taken for it might be easy to underestimate uncertainties introduced by such devices, for it is easy to misalign these axes as well as miss the losses introduced by multiple interfaces and vibrational deformations of the bearings.

Depending on the mounting technique, variance of measured spectra is expected. The goal of this test is to measure and, if possible, quantify this variance so it can be applied to overall response correction factor.

3.6.1 Test setup

Duraluminum fixture plate was used as a dummy test object for mount type tests. Following mounting options are considered, for these are the most common due to simplicity and ease of use:

- stud-bolt mount, where stud is cemented into bolt which screws into or through the test article;
- double-sided adhesive tape.

One accelerometer was used as a reference with screw-stud mounted directly onto shaker table (bolt fits into mount hole while fixing the interface plate to the shaker table). This reference is required for estimation of repeatability of these tests. Second accelerometer was used for measuring responses of different mounting options.

Setup was shaken at 5 ms^{-2} forced input with feedback measurement done on the fixture mount.

3.6.2 Test results

Test results indicate negligible difference between two mounting options in the range of interest. These small deviations can be explained by the change in accelerometer facing direction as well as the fact, that adhesive tape was applied over the stud hole, which reduces the total contact area and creates vibrations of the tape itself.

A side effect of this study was a discovery of insufficient stiffness of the shaker mounting table surface - it tends to experience natural mode vibrations and higher frequencies. Two orthogonal axes were chosen (X and Y) with cross-point at the centre of the table. In the center of the table feedback accelerometer was mounted, while multiple measurements were done with another accelerometer at different distances from center along both chosen axes. Figure 3.6.2 shows uncorrected measurement results as a function of distance from center. Thermal changes and small placement errors create slight discrepancies between signals, but overall trend can be noted by the visible grouping of the measurements according to the distance from the center. Opposite phases suggest approachment of first natural mode of center-fixed planar object. This conclusion does agree with documentation

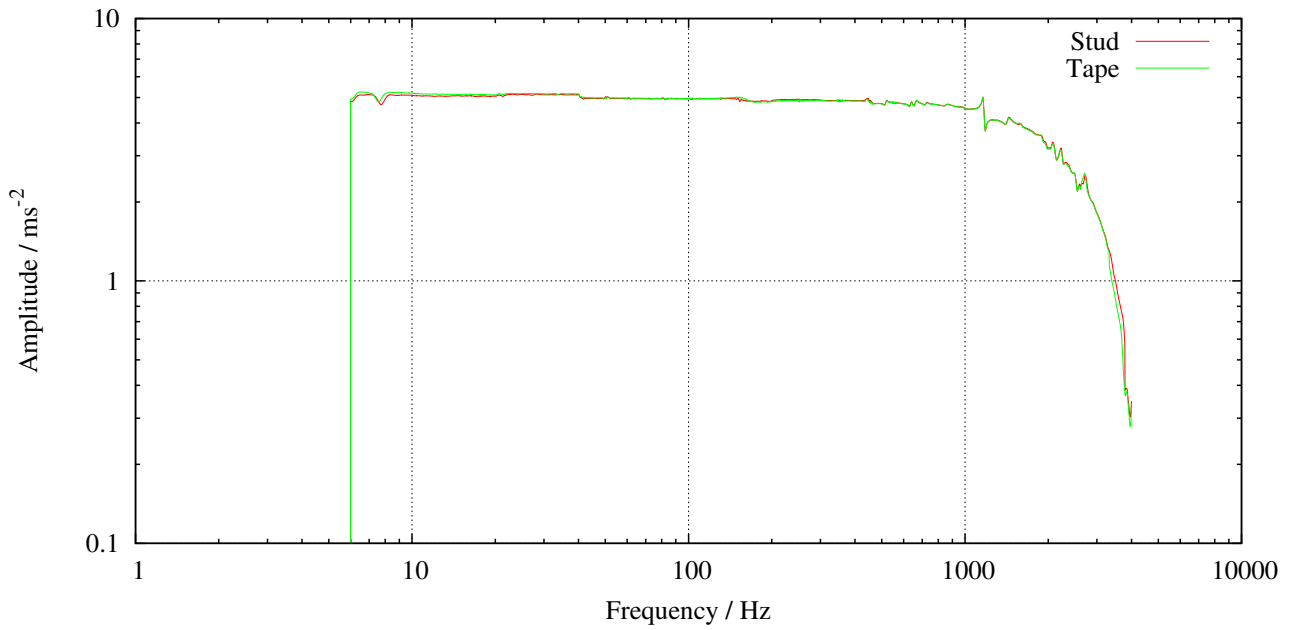


Figure 3.6.1: Comparison of stud-mounted and adhesive-tape mounted accelerometer responses

provided by the manufacturer, albeit natural response was expected to be much higher, to be outside the range of interest.

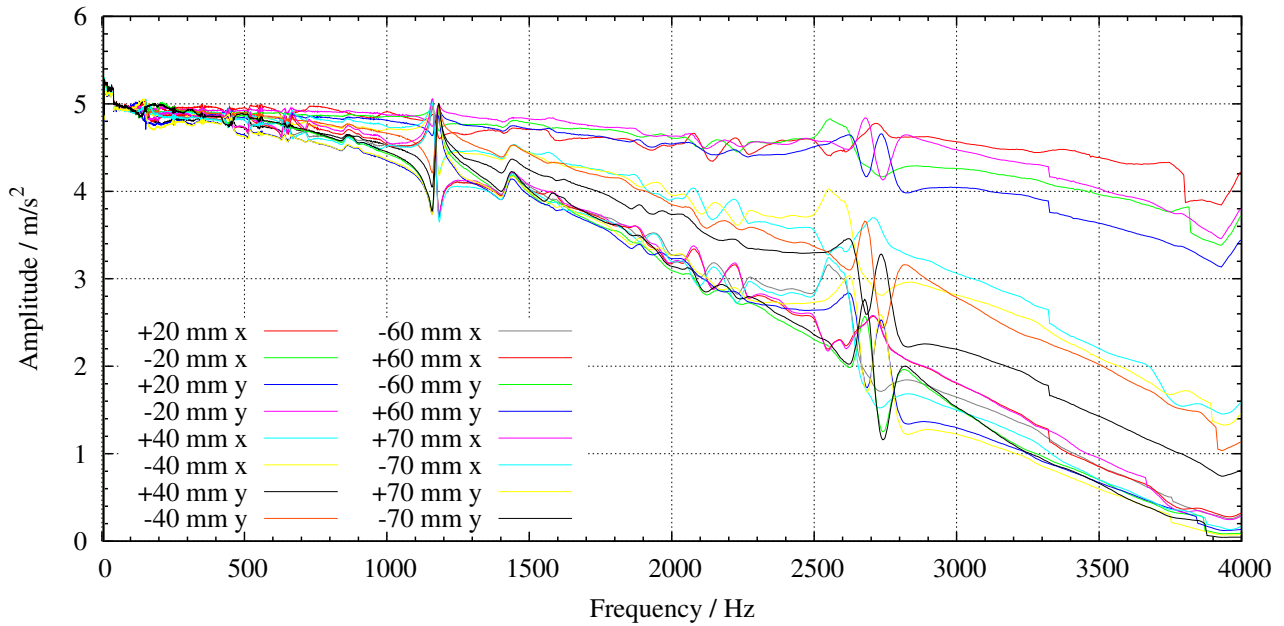


Figure 3.6.2: Uncorrected shaker table responses as a function of distance from center hole

3.7 Accelerometer placement influence on measurement output

Accelerometer placement on the DUT plays a large role in response measurement. Position of measurement is crucial to the results obtained due to following factors:

- off-axis sensitivity is low (within a range of couple percent), position should be chosen so that desired measuring direction coincides with the sensitivity axis;
- transducer should be located on the part of interest of DUT. Mounting on other parts, however closely they may be located and however tightly they might be coupled, still will make transducer pick up vibrations of other parts and experience sensitivity losses from desired part due to dampening in the joints;
- characteristics of vibration modes at different combinations of locations and exciting frequencies may differ grossly – a shift of just a couple of millimeters may result in moving from node to anti-node in some vibration modes. In frequency response spectrum it will appear as a sharp drop in amplitude in some of the minor harmonic peaks;
- rubbing of any part of measurement system with any part of DUT is highly unwanted. Not only it wears and damages all equipment and cabling involved, it also generates triboelectric noise.

These factors should be always kept in mind when performing tests on real articles. This test, however, is designed to estimate influence of modal shapes on the transducer output.

3.7.1 Test setup

An assembled ESTCube-1 printed circuit board was used as a mount point selection test object. Accelerometer mount spots were chosen in such a manner that different vibration modes can be observed while having high enough surface flatness to ensure minimal base strain and best adherence. For accelerometer placement test ESTCube-1 on-board computer model board was used in similar configuration as it is in assembled satellite - screw guided and separated by metal distancing tubes around the screw shaft. Having fixtures at corners of the board allows it to move in accordance with vibration modes. Locations of accelerometer mounting are shown in Figure 3.7.1. Components on the board limit the placement options (requirement of surface flatness is not fulfilled) and add localized stiffness to the board forbidding it to vibrate in some of its natural modes or drastically distorting these mode shapes. Constant acceleration profile of 9.8 ms^{-2} was applied and responses measured on the chosen points.

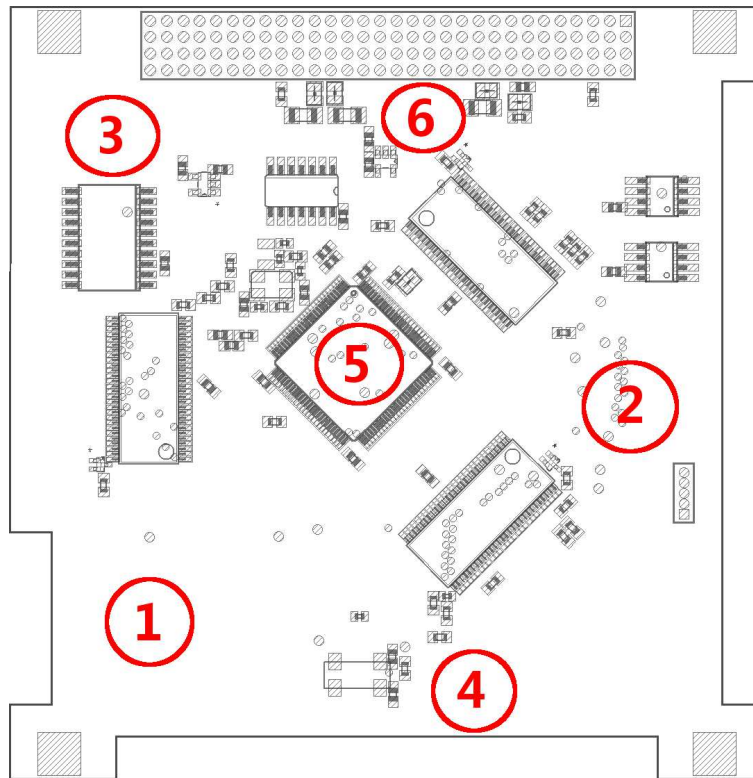


Figure 3.7.1: Drawing of the board used for accelerometer placement tests. Red circles mark chosen placements, with numbers indicating sequential number of measurement.

3.7.2 Test results

In case of frequency response dependency on the accelerometer placement, it changes as predicted - a complex system with many components each with their own stiffness matrix would vibrate differently at each point. Despite that main mode of the board itself at (350 ± 20) Hz remains clearly distinguishable, while minor modes are influenced heavily. Drift of main mode frequency can be seen in Figure 3.7.2 and is explained by mass loading, for mass of the assembled board is 48 g, while accelerometer is 5 g, which is below recommended minimum mass-ratio of 10 [41].

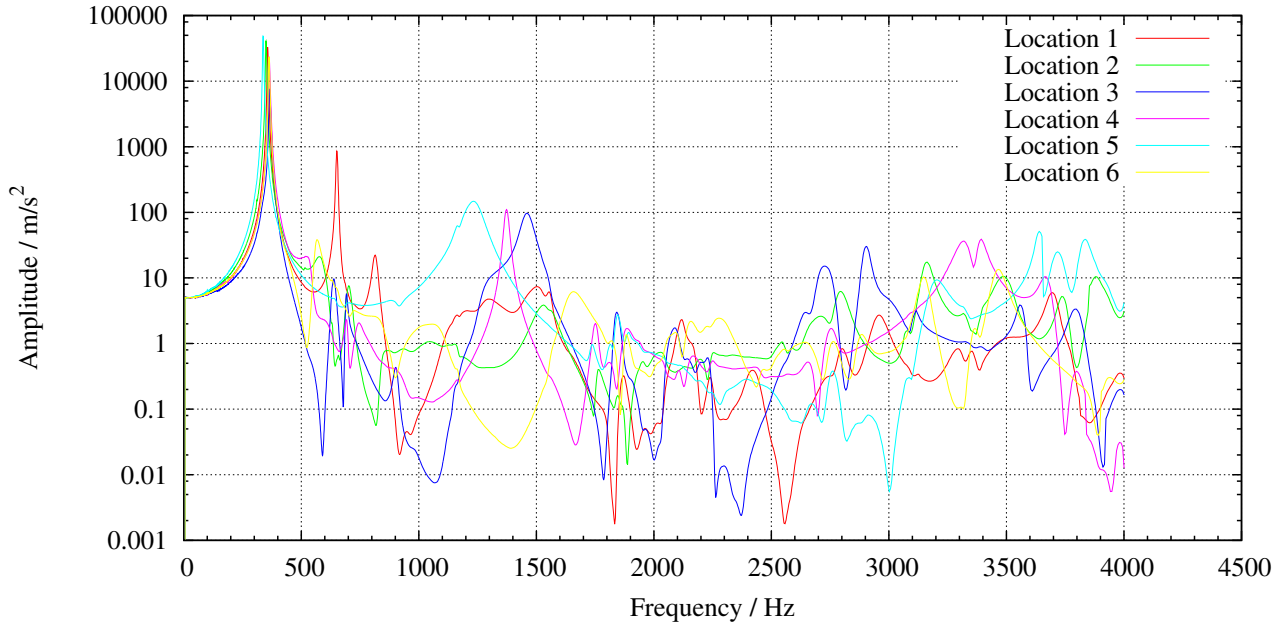


Figure 3.7.2: Uncorrected graphs of frequency response dependence on the accelerometer placement.

Results obtained during these tests confirm the necessity of finite element modeling (FEM). FEM allows to predict the response on any chosen spot on the DUT, vibration testing is used only to verify and/or correct models. Results also indicate the necessity to know exact point of interest, which should be supplied by the customer (owner of the test article).

3.8 Frequency response spectrum corrections

As discussed in previous chapters, there are quite a few parameters in both acquisition and measurement devices, which although linear, but variable never the less. In this section all of the aforementioned parameters will be joined together and applied to the measured spectra. Corrections to be applied are listed in Tables 3.8.1 and 3.8.2 for both accelerometers. Further in this text correction coefficients stated in calibration documentation will be named as c_{name} (note the lowercase 'c') and calculated values will be denoted using capital 'C' - C_{name} .

Change in sensitivity is expressed as a linear slope on logarithmic scale. While it is very convenient to calculate exact values for integral decades, it creates an additional calculation challenge for intermediate values or even partial values (frequencies measured sometimes are stated as two-digit decimal parts, especially on the low-frequency end of the spectrum) and the reference itself is stated at a partial value. To overcome this, frequency difference between reference point and measurement point has to be converted to logarithmic scale before used as multiplier for actual value calculation:

$$C_{sens} = \log_{10}\left(\frac{f_x}{f_{ref}}\right) \cdot c_{sens} \cdot S_{ref}. \quad (3.8.1)$$

Correction name	Correction value accelerometer A	Note
Sensitivity change (c_{sens})	-2.5 %/dec	Varies with frequency
Transverse noise (c_{trans})	5 % of reference sensitivity	Constant, worst case scenario taken
Inherent noise (c_{inh})	25 mm s ⁻² /√Hz for 10 Hz	Varies with frequency
	6 mm s ⁻² /√Hz for 100 Hz	
	3.5 mm s ⁻² /√Hz for 1 kHz	
Thermal correction (c_{temp})	+0.09 %/°C	Temperature-dependent
Measurement channel offset (c_{offs})	0.00018 V	Constant
Measurement channel gain error (c_{gain})	0 %	Constant

Table 3.8.1: List of correction factors for “Control” accelerometer [23].

Correction name	Correction value accelerometer B	Note
Sensitivity change (c_{sens})	-2.6 %/dec	Varies with frequency
Transverse noise (c_{trans})	5 % of reference sensitivity	Constant, worst case scenario taken
Inherent noise (c_{inh})	25 mm s ⁻² /√Hz for 10 Hz	Varies with frequency
	6 mm s ⁻² /√Hz for 100 Hz	
	3.5 mm s ⁻² /√Hz for 1 kHz	
Thermal correction (c_{temp})	+0.09 %/°C	Temperature-dependent
Measurement channel offset (c_{offs})	0.00028 V	Constant
Measurement channel gain error (c_{gain})	0 %	Constant

Table 3.8.2: List of correction factors for “Measurement” accelerometer [42].

C_{sens} should be negative when measured frequency f_x is lower than reference frequency f_{ref} , but positive for values higher than f_{ref} .

Transverse noise normally is a function of placement rotation angle. The direction of minimum sensitivity is indicated on the accelerometer body with a red dot. It is recommended to install it with least sensitive side aligned perpendicularly to the plane of highest expected transverse vibrations. In real-life measurements it is often difficult to predict transverse motion direction due to the limited knowledge of DUT construction peculiarities, so the worst case scenario is assumed:

$$C_{trans} = 0.05 \cdot S_{ref}. \quad (3.8.2)$$

Since reality often contradicts theory, there are no red dots on accelerometers. This implies that the direction of maximum transverse noise is not known and should be taken as uncertainty source with equal probability of being in any direction. Due to aforementioned factor, C_{trans} becomes u_{trans} :

$$u_{trans} = \frac{C_{trans}}{\sqrt{12}}. \quad (3.8.3)$$

Inherent noise or internal amplifier noise is given as an amplitude spectral density in terms of g/\sqrt{Hz} . In calibration chart manufacturer conveniently indicates noise figure for the whole range in microvolts. Since bandwidth is strictly test-dependent, for general use worst case broadband noise figure will be used (0.008 ms^{-2}).

Thermal correction requires ambient temperature to be known at the measurement time and place. Temperature difference between calibration and measurement is used to obtain numeric value:

$$C_{therm} = (|T_{ref} - T_{meas}|) \cdot C_{therm}. \quad (3.8.4)$$

Tartu Observatory laboratories have environmental control, meaning temperature and humidity are automatically adjusted to be at a constant level of $(21 \pm 1)^\circ\text{C}$ and $(50 \pm 10)\%$ relative humidity. During the vibration test, shaker and accompanying electronics generate a considerable amount of heat (more than ventilation system can withdraw). Positioning of shaker cooling fan is restricted by architecture, so it happens to blow warm air back in to the room itself. As a consequence of these factors, accumulation of heat happens. A digital thermometer sensor was placed next to shaker mounting table to measure ambient temperature changes as close to accelerometers as possible.

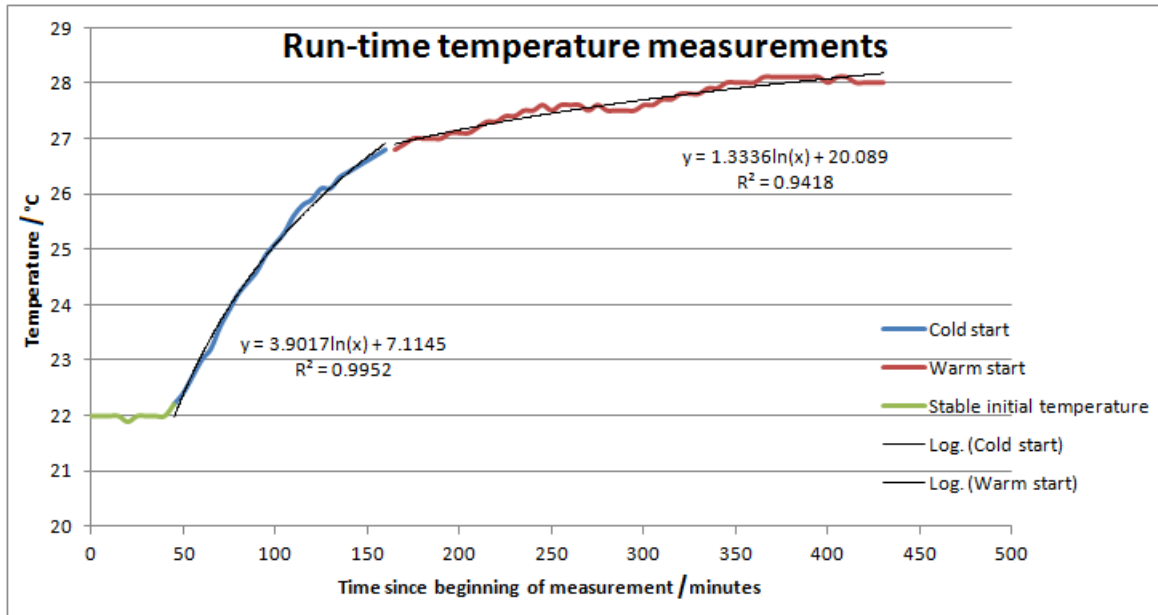


Figure 3.8.1: Temperature measurements during vibration test bench operations.

In figure 3.8.1 initial stabilized temperature which was kept by climatic control at a level of $\sim 22^\circ\text{C}$ is shown in green. To provide better temperature estimate, measurement was divided into two parts (*cold start* and *warm start*) with separated logarithmic fit curves for each. System was turned on for warm-up at time $t = 50$ minutes and left in this condition for about 150 minutes until $t = 200$ min. Actual testing began after that, giving system more than two hours for warming up. It should be noted, that no substantial increase in thermal output of the system was observed when comparing free-running (shaker not moving) to utilized system (shaker moves).

To apply these thermal corrections to measurement results, test engineer has to note time when the system has been turned on, when testing has been commenced and duration of each test. Planned correction script would have two variables - time of start of the test and duration. These two variables allow to choose correct fit curve to use and apply it to measurement results with estimated temperature changes.

Thermal transient sensitivity shall not be taken into account for in laboratory conditions thermal drifts are expected with frequency lower than stated 3 Hz (as measurements over last half a year indicate).

Measurement channel offset is zero-bias or measurement offset from zero. Assumed to be constant.

Measurement channel gain error is percentage value of inbuilt amplifier error. Assumed to be constant in-between calibration periods.

Cable attenuation is a factor of signal level losses within transmission cable. Due to the physical build of shielded cables, they are typically modeled as an RLC element and therefore have some electrical impedance. Stated capacitance is 100 pF/m and 50 ohm impedance at 100 MHz for cable type AC-0104. [43] indicates that cabling loss can be neglected, for impedance effects for given application frequency range are practically non-existent for cabling length below 100 feet (30 m). Special low noise cables with double shielding and lubricant-filled cables, when properly tied down do not produce any losses or triboelectric effects.

Amplitude measurement correction can be summarized incorporating all the aforementioned correction factors, which yields final correction equation for obtaining corrected amplitude $A_{corrected}$ from measured amplitude $A_{measured}$:

$$A_{corrected} = A_{measured} \pm C_{sens} + C_{temp} - C_{offs} - A_{measured} \cdot C_{gain}. \quad (3.8.5)$$

Eq.(3.8.5) has $\pm C_{sens}$ value for it is frequency-dependent - below reference frequency of 159.2 Hz it has to be subtracted, above reference frequency it has to be added.

Theoretically TEDS should enable automatic application of correction factors, but unfortunately “Type 7541” controller does not have TEDS support, so corrections have to be applied manually or using third-party software.

Final test results are to be presented as a frequency-amplitude graph. Test bench control software provides environment for live observation of the response measured, but does not offer a possibility to modify any input parameters to implement corrections needed or depict uncertainties. Control software offers a possibility to export measurements as CSV (comma-separated value) files which can be operated with. These files are written in form “<frequency>, <amplitude>, <newline>” and operations with such files are relatively common. Number of recorded samples (points per measurement) is presettable in software and limited by it up to 4096 points and determines the length of output file. Author is going to use PythonTM[44] scripting language for applying correction factors on measurement result data file and Gnuplot [45] software package for graph generation.

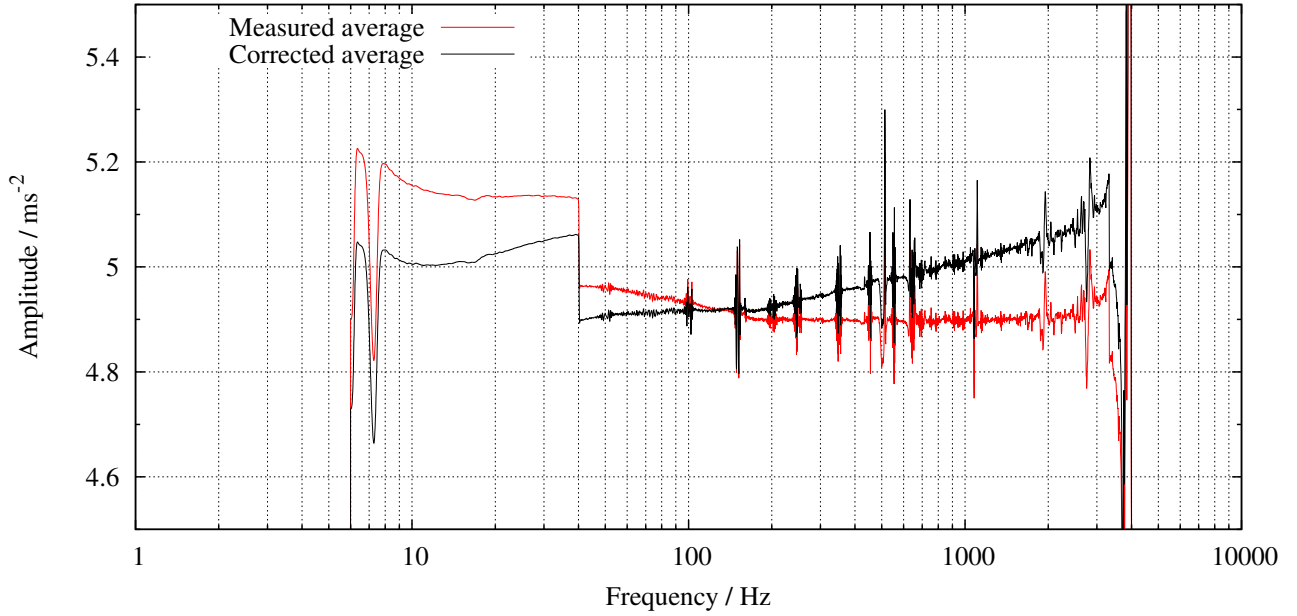


Figure 3.8.2: Repeatability test response spectra: measured spectrum plotted along with spectrum corrected for offsets and errors.

It can be seen in Figure 3.8.2 (zoomed in region of interest) that application of correction factors change the measurement result significantly (up to 0.2 ms^{-2} of 5 ms^{-2} average which is up to 4 % relative). While not critical at small amplitudes, difference in measured and corrected can be over 245 ms^{-2} at maximum range of 7000 ms^{-2} .

3.9 Uncertainty budget

For uncertainty estimation, electric equivalent of classic model (see Section 2.5) will be used, for a slightly modified version of such a chain is implemented in given case - signal sensing and conditioning are built into IEPE accelerometer, while filtering and FFT are done on the measurement device (controller). Uncertainty estimation is done in accordance with [46] recommendations. All the limited information available is used for evaluation of *Type B* error sources, while random effects are included as within-laboratory reproducibility.

3.9.1 Accelerometer contributions

It can be seen from the electric model depicted in Figure 2.5.3, that sensor consists of a charge source q_p with parasitic capacitance C_p and resistance R_p . These parasitic components are *virtual components*, meaning that they are not physically there, they are characteristic to the sensing element itself - they can be measured directly on the outputs of the sensing element. Due to the virtuality, these elements have no inherent errors or tolerances other than those imposed by measurement system. Same applies to interface cable capacitance C_c and amplifier input resistance R_i . Operational amplifier (op-amp) with its feedback components R_f and C_f , on the other hand, are real components with their manufacturing tolerances, drifts and other characteristics. In-depth analysis of op-amp circuit

parametric component tolerance impact on errors of amplifier output has been thoroughly described by [47]. Proprietary nature of accelerometer limits the amount of available information on its inner workings, namely types and tolerances of components used and exact schematic of the assembly. Manufacturer does provide some measured parameters related to amplifier circuitry with respective uncertainties:

Reference sensitivity expanded uncertainty is given as 1%, with coverage factor $k=2$, normal distribution. For calculation purposes all the uncertainty sources are normalized to standard uncertainty, which in this case means halving stated value, obtaining 0.5 % of reference.

Bias voltage or the *virtual ground* level about which AC measurement output can fluctuate is stated as $+12\text{ V} \pm 1\text{ V}$ at room temperature. This is input parameter and does not influence output uncertainty, for measurements are done about this value, which is exactly half of nominal supply voltage of $+24\text{ VDC} \pm 1\text{ V}$. Set and determined by transducer and controller automatically.

Output impedance is ability to drive load (ADC built into controller) without voltage distortion, given as $< 2\ \Omega$. This does not influence uncertainty of measurement, for ADC has input impedance of at least $500\text{ k}\Omega$, which is only a small fraction of transducer's drive ability.

Inherent noise, which was introduced in chapter 3.8 is amplifier noise, hence it is an uncertainty source in itself.

Temperature coefficient of sensitivity comes into play when correction factor is applied. Since correction factor is temperature-dependent, it is required to note the temperature with associated uncertainties. For laboratory environmental (temperature and humidity) measurements digital Comet D4141 thermo-hygro-barometer is used in logging mode. In calibration sheet stated uncertainty $u(t)_{cal}$ of RTD sensor is $0.21\text{ }^{\circ}\text{C}$ ($k=2$ with 95% confidence level) with $0.1\text{ }^{\circ}\text{C}$ resolution $u(t)_{res}$.

$$u(t) = \sqrt{u(t)_{cal}^2 + u(t)_{res}^2 + u(t)_{fit}^2} = \sqrt{(0.5 \cdot 0.21)^2 + \left(\frac{0.05}{\sqrt{3}}\right)^2 + u(t)_{fit}^2}. \quad (3.9.1)$$

If temperature measurement of whole test period is used, uncertainty of the temperature measurement fit function $u(t)_{fit}$ has to be incorporated into budget. This term can be omitted, when instantaneous temperature is measured, but this approach can be only used for short measurements or in case synchronized response and temperature measurements are done. A series of run-time temperature measurements were done and similar patterns between these measurements can be noted in Figure 3.9.1.

Measurement graphs are shown for periods when vibration test bench is turned on, with ambient temperature and cool-down periods removed. It can be seen, that temperature patterns have substantial increase at seemingly random times from cold-start. Different warm-up times have been tried out and change in temperature increase does not coincide with start of the test, in fact, in most of the cases tests have been running for some time before jump in thermal output happens. The similarity of

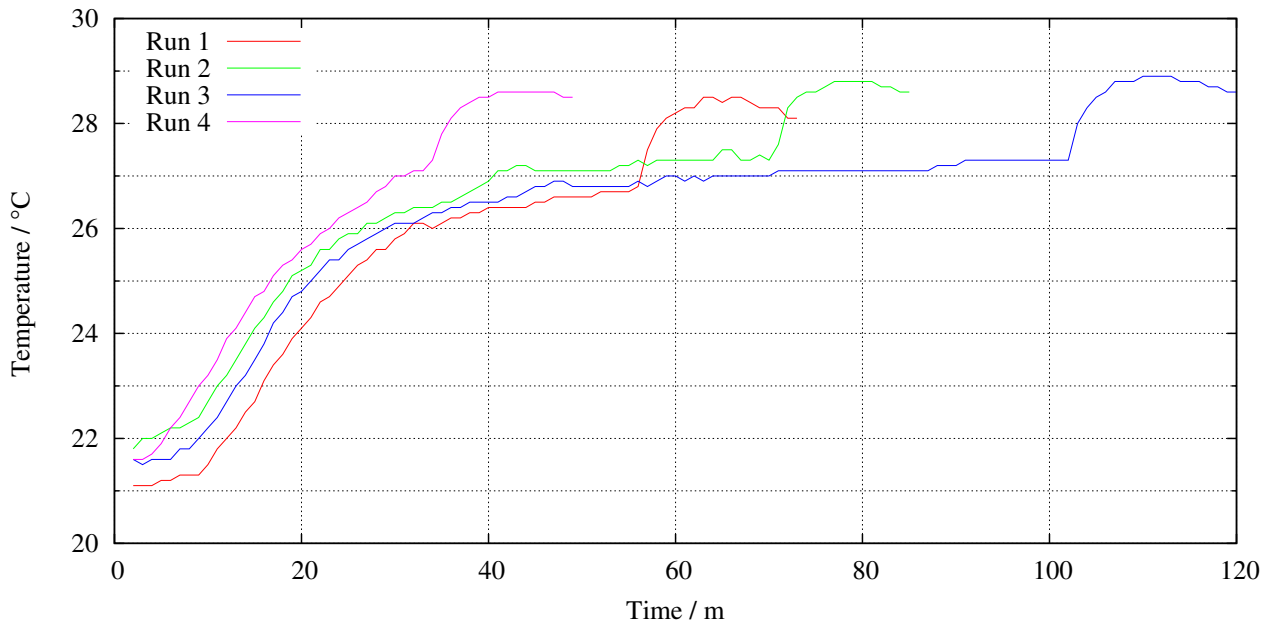


Figure 3.9.1: Change of the ambient temperature during the test.

slopes and heights of these jumps (they stop as suddenly as they started) looks very systematic. A possible explanation of this could be effect of resistance drop due increasing temperature, which in turn requires increase in power to generate more current. It could be that current limiter starts to operate at some point, thus limiting or stopping completely further increase in temperature. Another explanation of this phenomenon could be that for reasons unknown ventilation system stops operating for a limited amount of time, thus allowing for heat to accumulate within the room. Length of initial curve with may be dependent on the environmental conditions, mainly on the number of people and equipment running in the laboratory. Generally, this shape can be approximated with two to four separate logarithmic fitting curves, as described previously in Section 3.8. Reader may note lack of the characteristic “hook” in Figure 3.8.1, which is assumed to be due to increased duration of initial low-slope section.

Investigation of sources of these peculiar temperature graphs is not within the scope of this work, so they will be taken as a matter-of-fact and dealt with accordingly.

3.9.2 Measurement repeatability

Repeatability tests were performed on bare shaker with stud mounted accelerometers. Figure 3.9.2 shows frequency response spectra of five consecutive measurements in linear frequency scale. In this test setup accelerometers were stud-mounted side-by-side on the aluminum test fixture. Tests were run from cold-start uninterrupted all in the row, sweeping from 6 Hz to 4 000 Hz with constant acceleration of 9.80665 ms^{-2} . On primary ordinate axis measured frequency response of “measurement” accelerometer, which was mounted on the side of the shaker mounting table. On secondary ordinate axis amplitude standard deviation of these five measurements is plotted. It can be clearly seen at the beginning of the graph and especially well at around 3000 Hz frequency, that repeatability is an

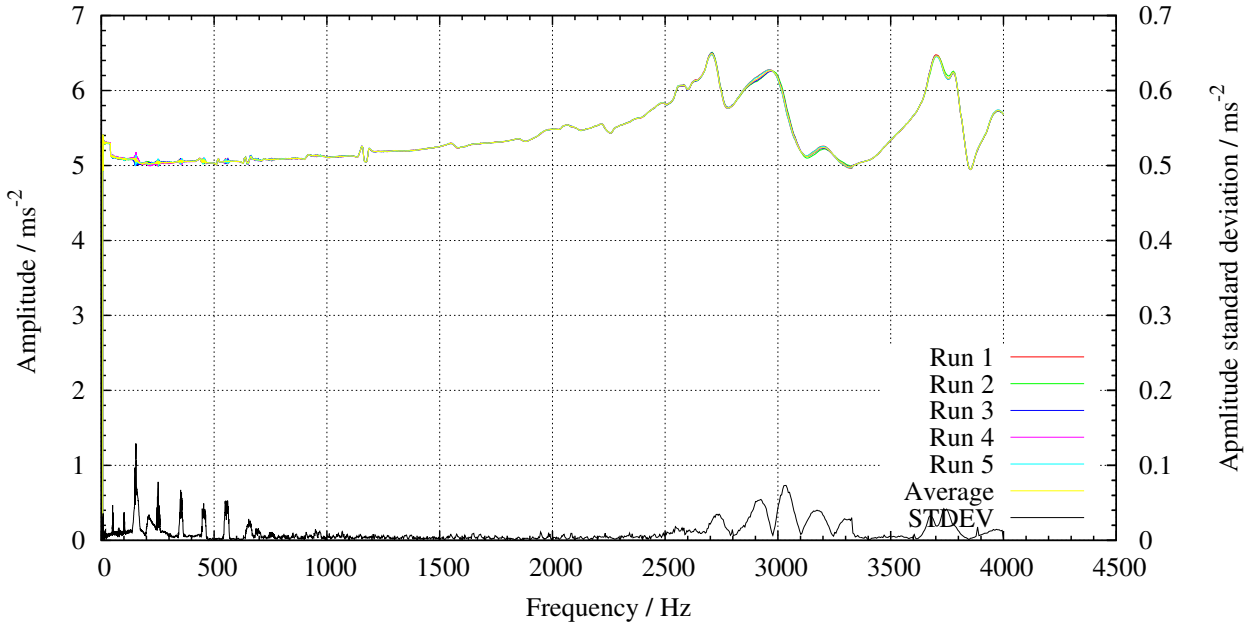


Figure 3.9.2: Frequency response spectra of 5 consecutive measurements after cold-start with standard deviation plotted on secondary y axis.

issue. It also can be seen that offsets vary, depending on frequency, so statistical analysis has to be performed step-by-step on each frequency separately.

Since in FRS measurements one has to deal with large amount of input data, author used Python™. A script (available in Appendix C.1) was created which performs mathematical operations on FRS CSV data files line-by-line. First, arithmetic mean value of five measurements (\bar{x}) was calculated in accordance with GUM [48] procedures:

$$\bar{x} = \frac{1}{N} \sum_{k=0}^N x_k. \quad (3.9.2)$$

where N is number of measurements, k is iterator and x_k is measured value. This mean value was used to obtain the variance of measurement results as an average sum of squared residuals:

$$s^2(x_k) = \frac{1}{N-1} \sum_{k=0}^N (x_k - \bar{x})^2. \quad (3.9.3)$$

Experimental standard deviation $\sigma(x_k)$ describes dispersion of observed values x_k about mean value \bar{x} was obtained from variance as a square root of it:

$$\sigma(x_k) = \sqrt{s^2(x_k)}. \quad (3.9.4)$$

Experimental standard deviation of the mean $\sigma(\bar{x})$ which commonly is accepted as *Type A standard uncertainty* was calculated from experimental variance of the mean:

$$u(x) = \sigma(\bar{x}) = \sqrt{\frac{\sigma^2(x_k)}{N}}. \quad (3.9.5)$$

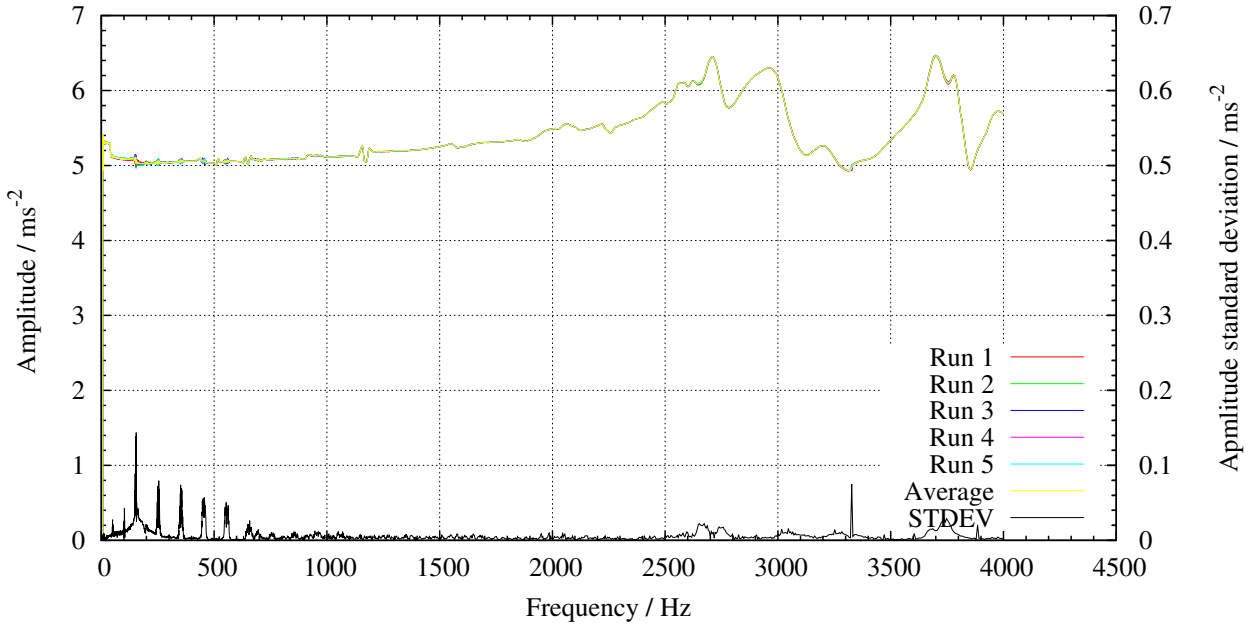


Figure 3.9.3: Graphs of 5 repeatability measurement set results run after a warm-up.

Figure 3.9.2 shows acceleration change up to 3 % relative to measured, on the single channel. Analysis of frequency response spectra as a ratio of input to output allows to reduce common signals arising from mount imperfections, thus lowering relative deviation values to 1% and below (see Appendix C.2 for more graphs). It was observed, that deviation values are dependent on the system temperature - measurements done after a warm-up are more stable than those performed right after cold-starting. Figure 3.9.3 depicts lower values and areas under peaks for warmed-up system than those seen in Figure 3.9.2, which is for cold-start.

3.9.3 Within laboratory reproducibility

Within laboratory reproducibility tests have been performed by author over period of multiple weeks. Reproducibility conditions were mainly the same over the whole measurement pool - same instruments with the same settings, same test article (aluminum test fixture with screw-stud mounted accelerometers). Even number of measurements was kept the same. Only variable parameters were temperature in the laboratory and test date/time. Time windows between sampling were at least one day, in most of the cases other tests were run in-between.

Simplified pooled standard deviation formula was used - without weighting factors, for sample sizes remained unchanged over the whole pool:

$$s_{pooled} = \sqrt{\frac{s_1^2 + s_2^2 + \dots + s_n^2}{n}}. \quad (3.9.6)$$

Measurement result graphs can be seen in Appendix B.2. Measurements were done in the form of transmissibility (or what in BKS software is denominated as Frequency Response Spectrum) - a ratio of feedback accelerometer output to measurement accelerometer output. This allows to neglect changes in environmental temperature, for these changes are incorporated in both transducers with

the same magnitude, thus effectively canceling each other out. Last figure in series is depicting pooled results (each “run” is actually a set of measurements with their own standard deviations). Pooled standard deviation was calculated, its mean value was calculated using trapezoid variation of Riemann sum approximation of area under the curve. This mean value was distributed evenly over the whole range to take into account accelerometer and DUT mounting imperfections.

3.9.4 Uncertainty budget summary

Total uncertainty can be graphically presented in the form of Ishikawa or *fishbone* diagram. All uncertainty components listed in Figure 3.9.4 are divided into four main parts - accelerometer, temperature measurement, input differential measurement and input analog-to-digital converter parts. Repeatability goes directly into main branch, meaning it directly influences final result.

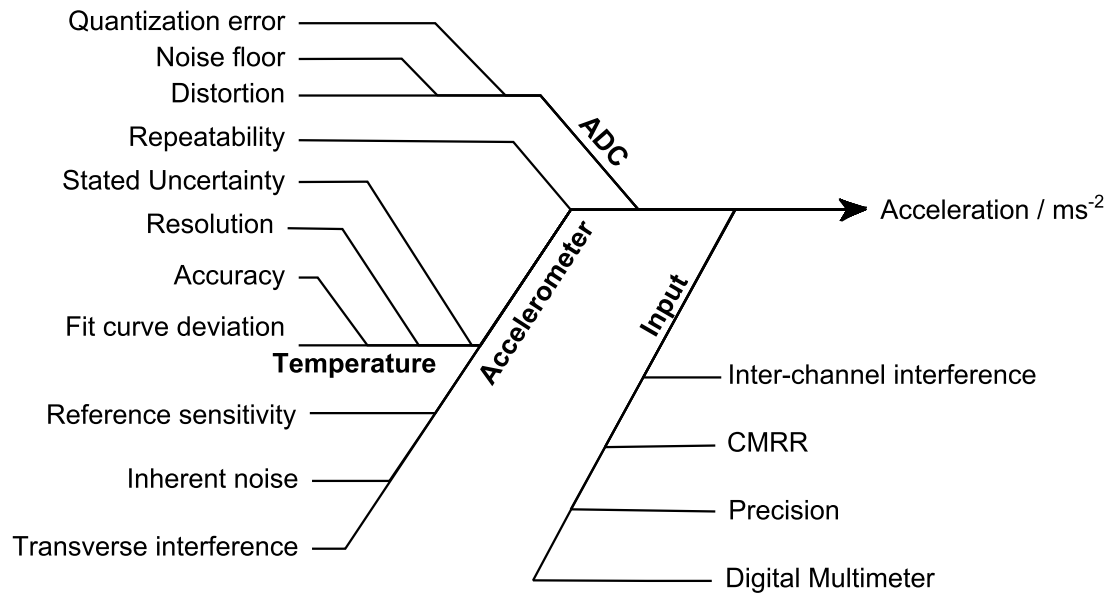


Figure 3.9.4: Uncertainty presented in form of Ishikawa diagram

While Ishikawa diagrams are useful for a quick overview, in-depth information typically is presented in the form of a table. All the uncertainty components are summed up in Table 3.9.1, which contains an example of uncertainty calculations for signal value measured with "measurement" accelerometer at frequency of 74.26 Hz:

Table 3.9.1: Vibration frequency response spectrum uncertainty budget contributors.

Quantity	Standard uncertainty	Probability distribution	Sensitivity coefficient	Uncertainty contribution
$u(f)$	0.8%	Gaussian	1	585 mHz
$\sigma(Q)_{DSP}$	0.34 μV	rectangular	0.9935	0 ms^{-2}
$\sigma(Q(x)_{eff})$	57.67 μV	rectangular	0.9935	0 ms^{-2}
σ_{CMMR}	0.06 μV	Gaussian	0.9935	0.06 ms^{-2}
u_{trans}	0.0049 ms^{-2}	rectangular	1	0.0049 ms^{-2}
$u(S_{ref})$	0.0005 ms^{-2}	rectangular	1	0.01 ms^{-2}
u_{temp}	0.09 $^{\circ}\text{C}$	rectangular	0.09	0 ms^{-2}
u_{repr}	0.0324 ms^{-2}	uniform	1	0 ms^{-2}
$u_{nonlinearity}$	0	Gaussian	1	0 ms^{-2}
u_{inh}	0.008 μV	Gaussian	0.9935	0.01 ms^{-2}
$u(DMM_{total})$	1.34 mV	rectangular	0.9935	0.4 ms^{-2}
Standard Uncertainty	-	Assumed Gaussian	-	0.4 ms^{-2}
Expanded Uncertainty	0.4 ms^{-2}	Assumed gaussian	2	0.8 ms^{-2}

Measurements, used for this example, had measured amplitude of 9.97 ms^{-2} which would make relative expanded uncertainty 0.8 %. Given singular result can be expressed as measurement result at (74.3 \pm 0.6) Hz with measured acceleration of (9.97 \pm 0.8) ms^{-2}

Total frequency-dependent uncertainty can be graphically presented as additional graph on secondary y-axis along with corrected response and overlain uncertainty. Figure 3.9.5 shows proposed way of depicting measurement results with non-corrected originally measured graph added for comparison. Latter can be removed, because end-user (client) does not need to know erroneous measurement values, only the traceable ones.

Largest sources of uncertainty are digital multimeter and reproducibility measurement uncertainties in this order. Digital multimeter alone contributes over 3%, while reproducibility measurements included most of the other error sources. When multimeter uncertainties are neutralized, the frequency-dependance of uncertainties becomes apparent in Figure 3.9.6.

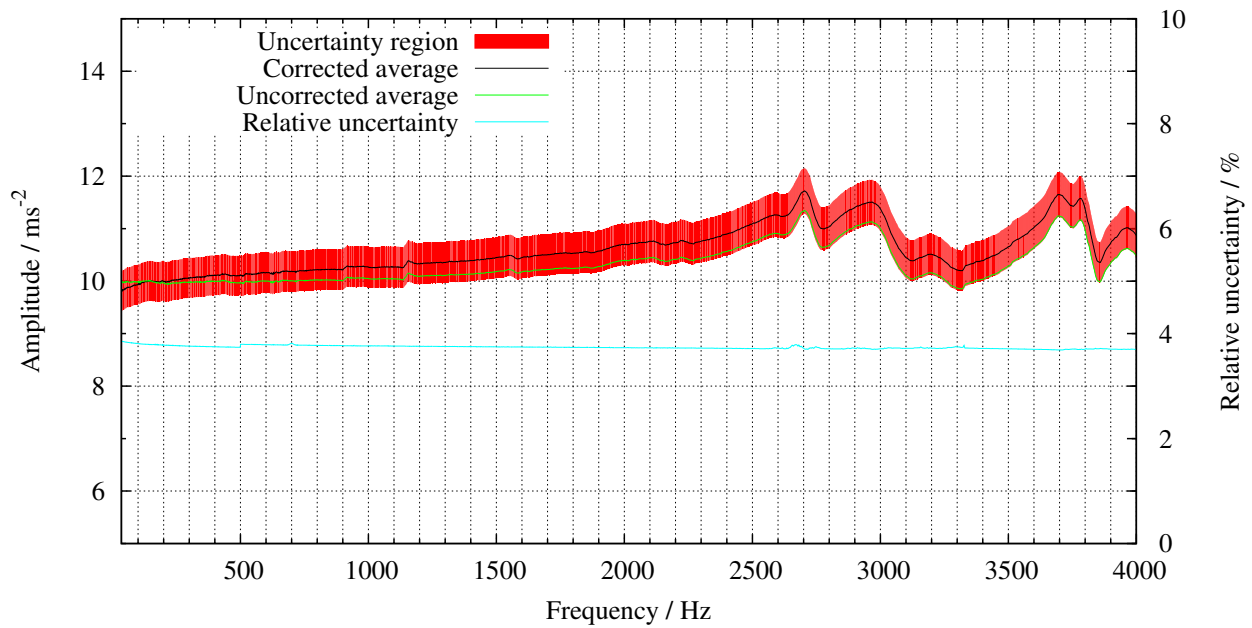


Figure 3.9.5: Corrected frequency response graph with uncertainties and uncorrected graphs shown.

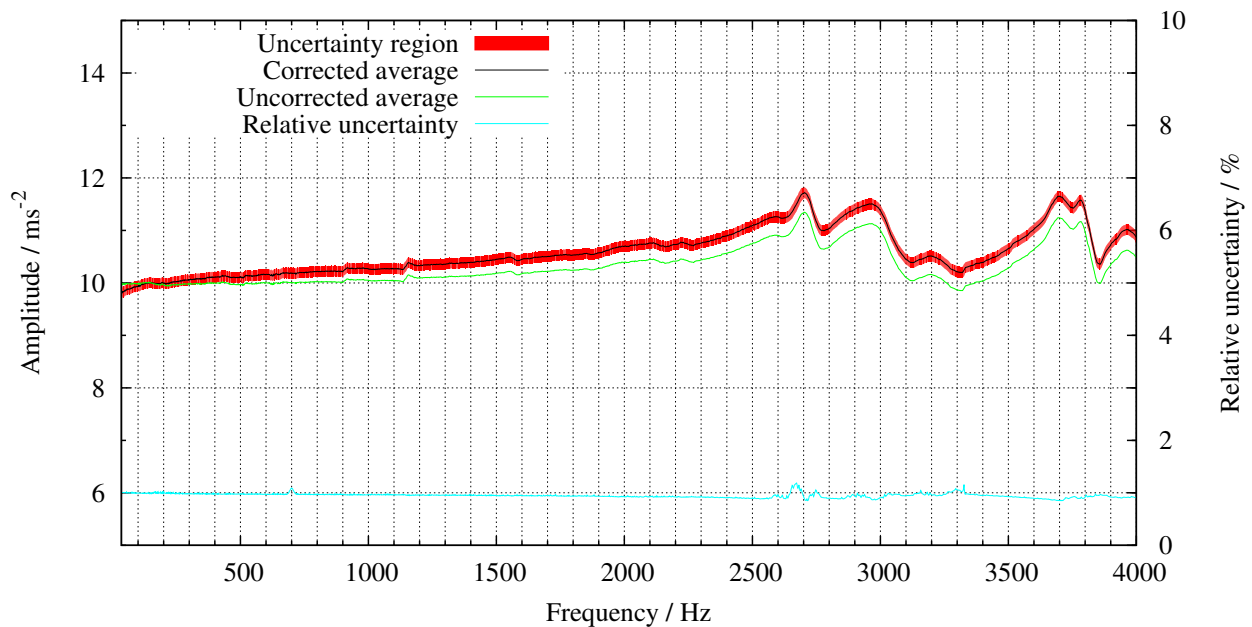


Figure 3.9.6: Corrected frequency response graph with uncertainties and uncorrected graphs shown. DMM influence removed completely for visualization purposes.

Chapter 4

Discussion and conclusions

A general framework of vibration frequency response measurement has been established. Analysis of the measurement system has revealed that initial assumption was correct - frequency response uncertainties, albeit on small scale, but do vary with frequency. Methods of testing and verification of vibration measurement system have been developed and tested. Practical application of these methods still require further development, main proposed improvements could be on instrumentation side - more accurate RMS amplitude measurement system alone could improve results three-fold. Thermal and sensitivity change corrections are main contributors to measurement result offsets which have to be corrected. It was proposed to laboratory administration to modify premises in such a manner, that allows proper disposal of the heat generated, which would improve reliability of measurements.

Format of the measurement results proposed is graph depicting corrected measurement results with uncertainties overlapping and shown separately on secondary axis as a relative value. Together with such graphical representation of amplitude uncertainty, statement about frequency uncertainty should be made. Author was unable to precisely quantify frequency uncertainties over the whole range, so proposed statement is “below 0.8% of measured frequency with coverage factor $k=2$ ”, which has been measured and evaluated, based on measurement results.

Joints and fixtures also play significant role on the measurement uncertainty - not only loose bolts and improper connections can cause additional unwanted peaks in responses (often with multiple harmonics), but even absence of spring washers makes bolts vibrate in their sockets by the distance equal to thread looseness. Improperly designed test article fixture will lack in stiffness and thus will introduce additional transverse or torsional vibrations.

Manufacturer's software provided with the system lacks some features related to uncertainty estimations. For example, digital signal processor works with large number of samples (Nyquist sampling theorem requires at least twice the frequency of interest), sometimes it even indicates sampling rate in range of multiple tens of kilohertz, as well as allows averaging of measurements on the fly, but it does not allow saving more than 4096 measurement points, nor does it provide simple statistics about these averages. Such low resolution defeats the purpose of low sweep rates, for results are often lost in large-scale resolution - roughly 4100 samples in full range of 5 Hz to 4 kHz in linear scale provides resolution step of 0.98 Hz. This could be related to minimum measurement filter bandwidth of 1.01 Hz.

As it was indicated in previous paragraphs, goals, established in Section 3.1 have been fulfilled:

1. a vibration system has been analyzed for sources of uncertainty;
2. generalized procedures for uncertainty budget compilation of accelerometer-based electro-mechanical vibration systems has been defined;
3. required corrections of measured signals have been established and applied in semi-automatized manner;
4. a method of reporting frequency-dependent measurement results and uncertainties in graphic form has been offered.

This work shall be continued with gradual improvements over time. Plans include, but are not limited to:

- reducing uncertainties arising from measurement instrumentation used in verification by using more accurate instruments when available;
- development of additional measurement and verification methods;
- creation of unified automated measurement system.

Summary

Vibration testing is a common practice for evaluation of equipment's ability to withstand operational environment vibrations, as well as verification of modal properties of equipment. Typically vibration test results state maximum uncertainty level for the whole test range or do not state it at all.

This study is an attempt to evaluate end-user test system error sources via application of equipment available in any R&D laboratory, namely signal generators and analyzers, oscilloscopes and digital multimeters. Test system is divided into separate blocks which are evaluated separately using information provided in specifications and calibration charts, as well as experimentally derived characteristics. Main goal is to ascertain as many error sources as possible and evaluate them numerically. Since many of these characteristics are frequency-dependent, uncertainty has to be stated separately for each frequency.

Given thesis provides basic introductory information on vibrations and test system available in Tartu Observatory. After establishing background, in-depth analysis of information provided by manufacturer is performed, followed by experimental deriving of some parameters of the system, such as input offset, linearity and reproducibility.

Results of this work contain correction factors to be applied to the measurement results as well as uncertainties associated. Python scripts are provided for semi-automation of application of these corrections to the measurement results, as well as for generating graphical measurement outputs (corrected frequency response spectra with overlaid uncertainty limits).

In conclusion additional ways of reducing overall uncertainty levels are provided.

Keywords: *vibration, uncertainty, correction factors*

References

- [1] A. Reinart, “Tartu observatooriumi arengukava 2008-2013.” Inside use document, 2008.
- [2] A. S. Elnashai, “Assessment of seismic vulnerability of structures,” *Journal of Constructional Steel Research*, vol. 62, pp. 1134–1147, 2006.
- [3] R. Bishop, *Vibration*. No. 0521296390, Cambridge University Press, London, 2 ed., 1979.
- [4] K. B. and R. Scanlan, “Resonance, tacoma narrows bridge failure, and undergraduate physics textbooks,” *American Journal of Physics*, vol. 2, no. 59, pp. 118–124, 1991.
- [5] The aircraft accident investigation board/Norway, “Report on the convair 340/580 In-paa aircraft accident north of hirtshals, denmark, on september 8, 1989.” Online: <http://www.aibn.no/rapport-02-1993-eng-pdf?pid=Native-ContentFile-File&attach=1>, 1993.
- [6] C. Lalanne, *Sinusoidal Vibration: Mechanical Vibration and Shock Analysis*, vol. 1. Wiley, 2 ed., 2010. ISBN 9780470611906.
- [7] A. G. Piersol and T. L. Paez, eds., *Harris’ Shock and Vibration Handbook 6th Ed.* McGraw Hill, 2010.
- [8] F. Wahl, G. Schmidt, and L. Forrai, “On the significance of antiresonance frequencies in experimental structural analysis,” *Journal of Sound and Vibration*, vol. 219, p. 379, 1999.
- [9] H. A. C. Tilmans, “Equivalent circuit representation of electromechanical transducers: I. lumped-parameter systems,” *Journal of Micromechanical Microengineering*, no. 6 (1996), pp. 157–176, 1995.
- [10] D. Giagopoulos, D.-C. Papadioti, C. Papadimitriou, and S. Natsiavas, “Bayesian uncertainty quantification and propagation in nonlinear structural dynamics,” in *Topics in Model Validation and Uncertainty Quantification, Volume 5* (T. Simmermacher, S. Cogan, B. Moaveni, and C. Papadimitriou, eds.), Conference Proceedings of the Society for Experimental Mechanics Series, pp. 33–41, Springer New York, 2013.
- [11] J. Wijker, M. H. M. Ellenbroek, and A. deBoer, “Characterization and synthesis of random acceleration vibration specifications,” in *4th ECCOMAS Thematic Conference on Computational Methods in Structural Dynamics and Earthquake Engineering* (V. P. M. Papadrakakis, N.D. Lagaros, ed.), (Kos Island, Greece), June 2013.

- [12] Z. Mao and M. Todd, "Statistical modeling of frequency response function estimation for uncertainty quantification," *Mechanical Systems and Signal Processing*, pp. 333–345, March 2013.
- [13] S. Adhikari, M. Friswell, K. Lonkar, and A. Sarkar, "Experimental case studies for uncertainty quantification in structural dynamics," *Probabilistic Engineering Mechanics*, pp. 473–492, February 2009.
- [14] J. P. Hessling, "A novel method of estimating dynamic measurement errors," *Meas. Sci. Technol.*, pp. 2740–2750, September 2006.
- [15] P. Michaelides and S. Fassois, "Experimental identification of structural uncertainty - an assessment of conventional and non-conventional stochastic identification techniques," *Engineering Structures*, pp. 112–121, May 2013.
- [16] G. Zhai, Y.-h. Chen, and W.-b. Ren, "Random vibration analysis of switching apparatus based on monte carlo method," *Journal of Zhejiang University SCIENCE A*, vol. 8, pp. 422–425, 2007.
- [17] B. Singha, A. Bisht, M. Pandit, and K. Shukla, "Nonlinear free vibration analysis of composite plates with material uncertainties: A monte carlo simulation approach," *Journal of Sound and Vibration*, vol. 324, pp. 126–138, July 2009.
- [18] S. Laborde and A. Calvi, "Spacecraft base-sine vibration test data uncertainties investigation based on stochastic scatter approach," *Mechanical Systems and Signal Processing*, pp. 69–78, July 2012.
- [19] M. Norouzi and E. Nikolaidis, "Efficient random vibration analysis using markov chain monte carlo simulation," *SAE Int. J. Mater. Manf.*, vol. 5, pp. 77–86, 2012.
- [20] Installation and operating manual, *V650 series vibrators*. LDS Test and Measurement, LDS Test and Measurement, 2 ed., 1995.
- [21] Installation and operating manual, *Field power supply FPS10L*. LDS Test and Measurement, 1 ed., 1996.
- [22] Installation and operating manual, *PA500/1000L-CE Amplifiers*. LDS Test and Measurement, Baldrock Road, Royston, Herts SG8 5BQ, England, 1 ed., 1996.
- [23] Calibration Chart, "Calibration Chart for DeltaTron Accelerometer SN 30402, Brüel & Kjær Sound & Vibration Measurement A/S," 2012.
- [24] User manual, *Vibration Controller Types 7541 and 7542*. Brüel & Kjaer Sound & Vibration Measurement A/S, DK-2850 Nørum, Denmark, 4 ed., 2013.
- [25] Mixed-Mode Communication Working Group, "IEEE P1451.4 - A Smart Transducer Interface for Sensors and Actuators - Mixed-mode Communication Protocols and Transducer Electronic Data Sheet (TEDS) formats."

- [26] P. Thampi, J. Singh, M. M. Nayak, K. Rajanna, and M. S. Kumar, "Design and optimization of bulk micromachined accelerometer for space applications," *International Journal on Smart Sensing and Intelligent Systems*, vol. 1, pp. 1019–1030, December 2008.
- [27] H. W. Ott, *Noise reduction techniques in electronic systems*. John Wiley and sons, 2nd ed., 1988.
- [28] M. B. Weissman, "1f noise and other slow, nonexponential kinetics in condensed matter," *Reviews of Modern Physics*, vol. 60, pp. 537–571, April 1988.
- [29] IEEE Computer Society, "IEEE 754-2008 IEEE Standard for Floating-Point Arithmetic," 2008. doi: 10.1109/IEEESTD.2008.4610935.
- [30] D. Asta and F. Irons, "Dynamic error compensation of analog-to-digital converters," *The Lincoln Laboratory Journal*, vol. 2, pp. 162–182, 1989.
- [31] W. A. Kester, ed., *Data Conversion Handbook*. Elsevier, 2005. ISBN: 0-7506-7841-0.
- [32] E. C. Ifeachor and B. W. Jervis, *Digital Signal Processing: A Practical Approach*. Pearson Education LTD, 2 ed., 2002. ISBN-10: 0-201-59619-9.
- [33] W. G. Jung, ed., *Op Amp Applications Handbook*. Elsevier, 2005. ISBN 0-7506-7844-5.
- [34] SpectraCom Technical Specifications, "Gps-88 & gps-89 gps-controlled frequency standards," 2012.
- [35] K. Jaldehag, "Verification of a gps-controlled frequency standard, fluke model 910r or pendulum model gps-89 (translation from the original report no. femf016992 in swedish)," tech. rep., Swedish National Testing and Research Institute, 2000.
- [36] Product Data Sheet BP 0587-14, "Sine/noise generators types 1049 and 1051."
- [37] L. Tan and J. Jiang, *Fundamentals of Analog and Digital Signal Processing*. AuthorHouse, 2nd ed ed., 2008. ISBN: 978-I-43435641-3.
- [38] User's and Service Guide, *Agilent U1241B and U1242B Handheld Digital Multimeters*. Agilent, 2013.
- [39] "Ea-4/02 m: 2013. evaluation of the uncertainty of measurement in calibration," October. Available online: <http://www.european-accreditation.org/publication/ea-4-02-m>.
- [40] A. Chu, "Tp 291: Accelerometer selection based on applications," tech. rep., ENDEVCO, 2006. Available online: <https://www.smtnet.com/library/files/upload/TP291.pdf>.
- [41] O. Dossing, "Prediction of transducer mass-loading effects and identification of dynamic mass," in *Proceedings of the Ninth International Modal Analysis Conference*, pp. 306–312, 1991.
- [42] Calibration Chart, "Calibration Chart for DeltaTron Accelerometer SN 30403. Brüel & Kjær Sound & Vibration Measurement A/S," 2012.

- [43] B. Lent, “Practical considerations of accelerometer noise (imac xxviii),” tech. rep., MEGGITT, 2009.
- [44] “Python.” <https://www.python.org/>. [Online; accessed April-2014].
- [45] “Gnuplot.” <http://www.gnuplot.info>. [Online; accessed April-2014].
- [46] Nordtest, “Vibration measuring instrumentation: Verification procedure (nt acou 094),” Tech. Rep. UDC 628.517, Nordtest, 1995. ISSN 0283-7145.
- [47] R. Mancini, “Worst-case design of op amp circuits,” *Analog Applications Journal*, no. 2, pp. 42–46, 2002.
- [48] Joint Committee for Guides in Metrology, “Evaluation of measurement data - guide to the expression of uncertainty in measurement,” September 2008.

Kokkuvõte

Vibratsioonikindluse testimine on tavaline praktika, et kontrollida seadme vastupidavust selle töökeskkonnas esinevale vibratsioonile. Mõnikord, kuid mitte alati, esitatakse vibratsioonikatsete tulemustes ka hinnang katse läbiviimisel tekkivale määramatusale.

Antud töös püütakse anda hinnang võimalikele vibratsioonikatsete käigus tekkivatele mõõtevigadele kasutades suhteliselt lihtsalt kättesaadavat mõõteaparatuuri nagu signaaligeneraator, ostsilloskoop ja digitaalne multimeeter.

Katsesüsteem on jagatud erinevatesse plokkidesse, millest igaüht on analüüsitud eraldi, kasutades nii tootja poolt esitatud spetsifikatsioone ja kalibratsioonitabeleid, kui ka eksperimentaalselt määratud karakteristikuid. Töö eesmärgiks on määratleda kõik teadaolevad veaallikad ja hinnata nende mõju numbrilisel kujul. Kuna paljud neist parameetritest sõltuvad sagedusest, on vajalik mõõtemääramatused esitada iga sageduse jaoks eraldi.

Antud töös esitatakse kõigepealt sissejuhatav informatsioon vibratsiooni kohta, samuti kirjeldatakse Tartu Observatooriumis kasutatavat vibratsioonikindluse katsesüsteemi. Järgnevalt analüüsitakse põhjalikumalt süsteemi koosseisus olevate seadmete tootjate poolt kättesaadavat informatsiooni ning eksperimentaalselt mõõdetud süsteemi karakteristikuid nagu sisendparameetrite nihe, lineaarsus ja katsete korratavus.

Töö tulemuseks on mõõtetulemuste täpsuse parandamist võimaldavad korrektsioonitegurid, ja neile vastavad mõõtemääramatused. Programmeerimiskeeles Python on koostatud ka vajalikud tarkvarakomponendid saadud korrektsioonide ja määramatuste efektiivseks rakendamiseks vibratsioonikatsete tulemuste esitamisel. Need võimaldavad ka esitada katsetulemusi graafilisel kujul (korrigeeritud sagedusspekter koos mõõtemääramatuse põhjal arvutatud piirväärtustega).

Töö kokkuvõttes on esitatud ka soovitusel täiendavateks meetmeteks katsesüsteemi täpsuse parandamiseks.

Võtmesõnad: *vibratsioon, mõõtemääramatus, korrektsioonitegurid*

Acknowledgments

First of all, I would like to thank my girlfriend Õie Nikkel for being patient and putting up with me during the hectic time of writing this.

Then I would like to thank my supervisor Ph.D. Riho Vendt and Ph.D. Mart Noorma for providing an opportunity to be here and do what I do.

I would also like to thank Viljo Allik for all the technical support he has provided over time and especially for the translation of the summary. I would also like to thank Kungla community for being there and leaving me alone to write this thesis. Thanks, guys.

And last, but not least, I would like to thank whichever divine beings for being done with this. It's been a massive pain, but I learned a LOT.

This research was supported by European Social Fund's Doctoral Studies and Internationalization Programme DoRa.

Appendix A

Calibration sheets

A.1 Accelerometer calibration sheets

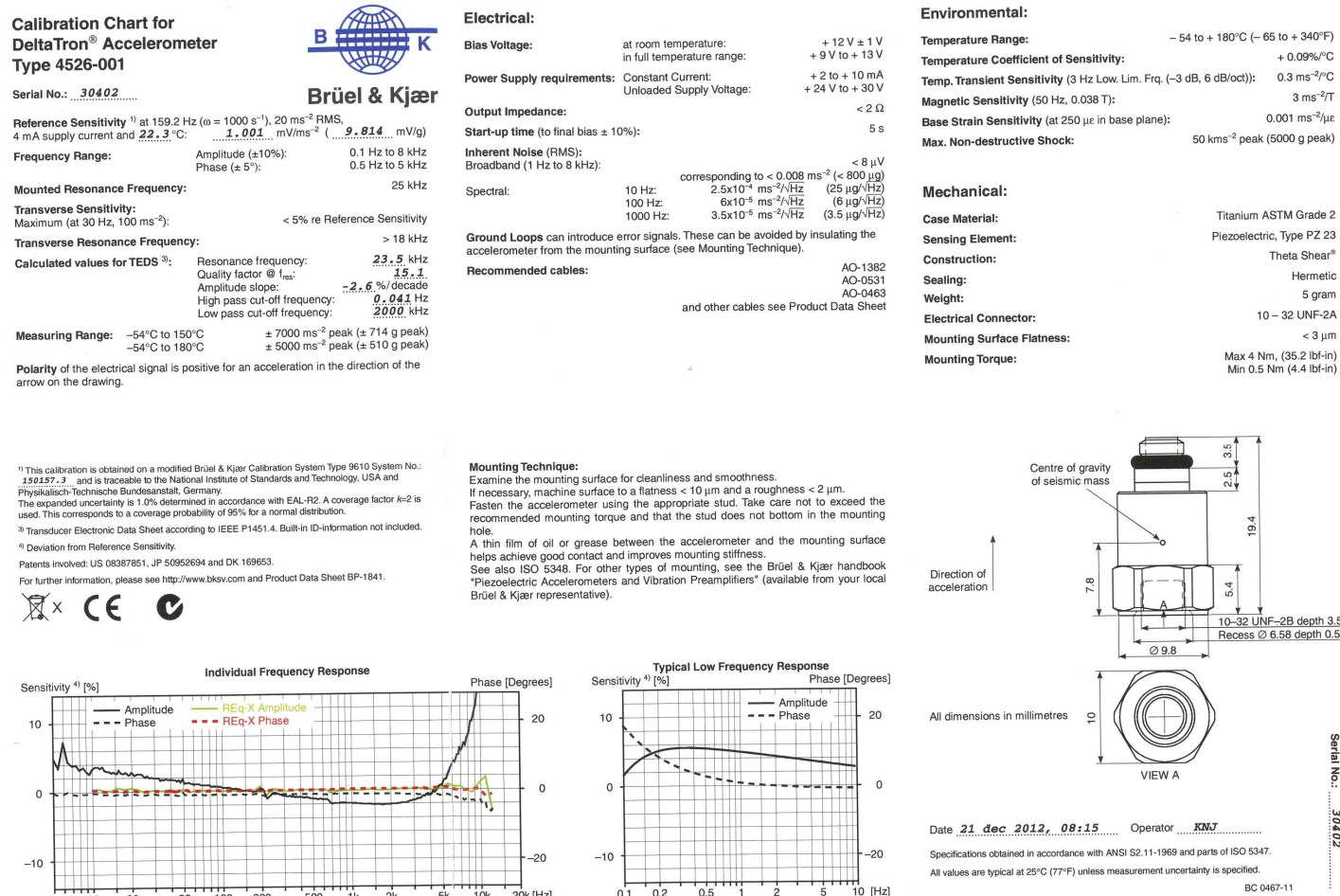


Figure A.1.1: Feedback accelerometer calibration sheet.

Calibration Chart for DeltaTron® Accelerometer Type 4526-001

Serial No.: 30403



Reference Sensitivity ¹⁾ at 159.2 Hz ($\omega = 1000 \text{ s}^{-1}$), 20 ms^{-2} RMS:
4 mA supply current and **22.2** °C: **0.9935** mV/ms² (**9.743** mV/g)

Frequency Range: Amplitude ($\pm 10\%$): 0.1 Hz to 8 kHz
Phase ($\pm 5^\circ$): 0.5 Hz to 5 kHz

Mounted Resonance Frequency: 25 kHz

Transverse Sensitivity:
Maximum (at 30 Hz, 100 ms⁻²): < 5% re Reference Sensitivity

Transverse Resonance Frequency: > 18 kHz

Calculated values for TEDS ³⁾: Resonance frequency: **24.0** kHz
Quality factor @ f_{res} : **25.5**
Amplitude slope: **-2.5** %/decade
High pass cut-off frequency: **0.011** Hz
Low pass cut-off frequency: **1548** kHz

Measuring Range: -54°C to 150°C $\pm 7000 \text{ ms}^{-2}$ peak ($\pm 714 \text{ g}$ peak)
-54°C to 180°C $\pm 5000 \text{ ms}^{-2}$ peak ($\pm 510 \text{ g}$ peak)

Polarity of the electrical signal is positive for an acceleration in the direction of the arrow on the drawing.

Electrical:

Bias Voltage: at room temperature: +12 V \pm 1 V
in full temperature range: +9 V to +13 V

Power Supply requirements: Constant Current: +2 to +10 mA
Unloaded Supply Voltage: +24 V to +30 V

Output Impedance: < 2 Ω

Start-up time (to final bias $\pm 10\%$): 5 s

Inherent Noise (RMS): < 8 μV

Broadband (1 Hz to 8 kHz): corresponding to < 0.008 ms⁻² ($< 800 \mu\text{g}$)

Spectral: 10 Hz: $2.5 \times 10^{-4} \text{ ms}^{-2}/\sqrt{\text{Hz}}$ ($25 \mu\text{g}/\sqrt{\text{Hz}}$)
100 Hz: $6 \times 10^{-5} \text{ ms}^{-2}/\sqrt{\text{Hz}}$ ($6 \mu\text{g}/\sqrt{\text{Hz}}$)
1000 Hz: $3.5 \times 10^{-5} \text{ ms}^{-2}/\sqrt{\text{Hz}}$ ($3.5 \mu\text{g}/\sqrt{\text{Hz}}$)

Ground Loops can introduce error signals. These can be avoided by insulating the accelerometer from the mounting surface (see Mounting Technique).

Recommended cables: AO-1382
AO-0531
AO-0463
and other cables see Product Data Sheet

Environmental:

Temperature Range: -54 to +180°C (-65 to +350°F)
Temperature Coefficient of Sensitivity: +0.0
Temp. Transient Sensitivity (3 Hz Low Lim. Freq. (-3 dB, 6 dB/oct)): 0.3 n
Magnetic Sensitivity (50 Hz, 0.038 T): 3
Base Strain Sensitivity (at 250 μe in base plane): 0.001 n
Max. Non-destructive Shock: 50 kms⁻² peak (6000 g)

Mechanical:

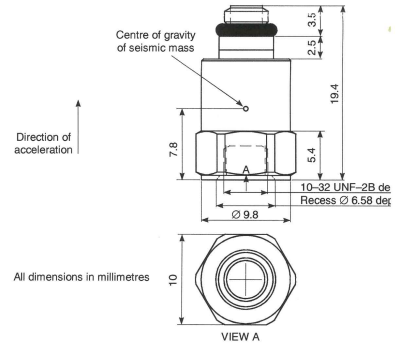
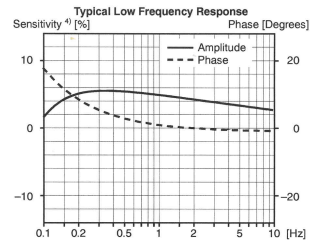
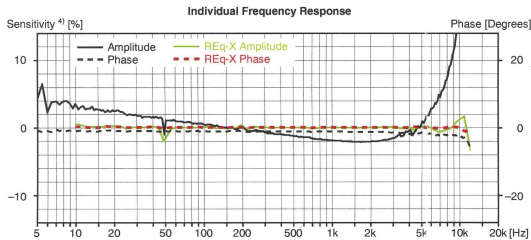
Case Material: Titanium ASTM G
Sensing Element: Piezoelectric, Type
Construction: Theta ξ
Sealing: He
Weight: ξ
Electrical Connector: 10 - 32 U
Mounting Surface Flatness: -
Mounting Torque: Max 4 Nm, (35.2
Min 0.5 Nm (4.4

¹⁾ This calibration is obtained on a modified Brüel & Kjær Calibration System Type 9610 System No.: 150157.3 and is traceable to the National Institute of Standards and Technology, USA and Physikalisch-Technische Bundesanstalt, Germany.
The expanded uncertainty is 1.0% determined in accordance with EAL-R2. A coverage factor $k=2$ is used. This corresponds to a coverage probability of 95% for a normal distribution.
²⁾ Transducer Electronic Data Sheet according to IEEE P1451.4. Built-in ID-information not included.
³⁾ Deviation from Reference Sensitivity.
Patents involved: US 06367851, JP 50952694 and DK 169653.
For further information, please see <http://www.bkav.com> and Product Data Sheet BP-1841.



Mounting Technique:

Examine the mounting surface for cleanliness and smoothness.
If necessary, machine surface to a flatness < 10 μm and a roughness < 2 μm .
Fasten the accelerometer using the appropriate stud. Take care not to exceed the recommended mounting torque and that the stud does not bottom in the mounting hole.
A thin film of oil or grease between the accelerometer and the mounting surface helps achieve good contact and improves mounting stiffness.
See also ISO 5348. For other types of mounting, see the Brüel & Kjær handbook "Piezoelectric Accelerometers and Vibration Preamplifiers" (available from your local Brüel & Kjær representative).



Date **21 dec 2012, 08:16** Operator **KNU**
Specifications obtained in accordance with ANSI S2.11-1969 and parts of ISO 5347.
All values are typical at 25°C (77°F) unless measurement uncertainty is specified.
BC 0467-11

Figure A.1.2: Measurement accelerometer calibration sheet.

A.2 Vibration controller calibration sheet

December-11-2012 15:35:12

Operation Information
Product Name: Type 7541
Manufacturer: Brüel & Kjær
Meter Model: Agilent 34401A
Last Calibrated Date: December-11-2012
Due for Calibration: June-18-2014
Hardware Version: 3.4.2
Firmware Version: 23110715

Product Serial Number: 1302400
Operator: Frank Wiese
Meter Serial Number: MY470183
Remark:
BIT Version: 30203
DSP Application Version: 3.2.4.6
PCB ID: 40075

Output Errors before Calibration

Channel ID	Calibration Range	Offset	Gain Error
Output 1	10v	-0,00096 V	-0,34 %
Output 1	0.1v	-0,00011 V	-15,96 %

Input Errors before Calibration

Channel ID	Calibration Range	Offset	Gain Error (Compare to full range)
Input 1	20v	0,03373 V	4,00 %
Input 1	0.2v	0,00012 V	1,00 %
Input 2	20v	0,01650 V	4,00 %
Input 2	0.2v	0,00233 V	1,00 %
Input 3	20v	0,06121 V	4,00 %
Input 3	0.2v	0,00002 V	1,00 %
Input 4	20v	0,07054 V	5,00 %
Input 4	0.2v	0,00023 V	1,00 %

Validated Gain and Offset Errors after Calibration

Offset Range:0.2v

Gain Range:20v

Channel ID	Offset	Gain Error	Results
Output 1	0,00001 V	0,0 %	Pass
Input 1	0,00018 V	0,0 %	Pass
Input 2	0,00028 V	0,0 %	Pass
Input 3	0,00033 V	0,0 %	Pass
Input 4	0,00010 V	0,0 %	Pass

Figure A.2.1: Vibration controller calibration sheet.

A.3 Vibration controller input specifications

Specifications – Input Channels

	7541	7542
Input Channels	2 or 4	4, 6 or 8
Input Connectors	4 x BNC	8 x BNC
Frequency Range	DC to 46kHz with 54 cutoff frequencies	
A/D Conversion	2 x 24 bit	
Data Transfer	24 bit	
Input Voltage Range	$\pm 20V_{max}$	
Input Signal Coupling	<i>Differential:</i> Signal ground is "floating" (500k Ω re chassis) <i>Single-ended:</i> Signal ground is connected to chassis ("grounded")	
Input Impedance	<i>Differential:</i> 1M Ω <i>Single-ended:</i> 500k Ω	
Absolute Maximum Input	$\pm 40V_{max}$ without damage	
High-pass Filters	<i>AC Coupling:</i> Analog high-pass filters, -3 dB at 0.3 Hz and -0.1 dB at 0.7 Hz Digital high-pass filters, user programmable	
Absolute Amplitude Precision, 1kHz, $1V_{input}$	0.5% FS	
Spurious-free Dynamic Range re Full-scale Input (Input terminated by 50 Ω or less) Spurious-free Dynamic Range is defined as the ratio of the rms full-scale amplitude to the rms value of the largest spurious spectral component (non-harmonic)	130dB typical	
Harmonic Distortion (all harmonics) Plus Noise	-100dBfs (DC to 1kHz) typical	
Crosstalk: Between any two channels of a module	< -100dB typical	
Channel-to-Channel Match ($10V_{max}$ input range)	<i>Max. Gain Difference:</i> 0.1dB typical <i>Max. Phase Difference:</i> < ± 1.0 degree, up to 20kHz	
Common Mode Rejection in $10V_{max}$ input range	> 90dB typical	
Anti-aliasing Filter (At least 90dB attenuation of those frequencies which can cause aliasing)	<i>Filter Type:</i> 3rd order Butterworth -3 dB @ 47kHz Slope: -18dB/octave	
Supply for DeltaTron/ICP [®] /CCLD	4 to 5mA from 21V source	
Charge Conditioning	10000pC and 49000pC with two stages	
Analog Special Functions	<i>Analog Self-test:</i> Functional check <i>Transducers:</i> Supports IEEE 1451.4-capable transducers with standardized TEDS (Type 7542 only: up to 30m cable length) <i>Versions and Templates Supported:</i> Contact Brüel & Kjær for a complete list	
Overload Detection	<i>CCLD Overload:</i> Detection of cable break or short-circuit + detection of CCLD transducer working point fault	

Figure A.3.1: Excerpt from vibration controller user manual with system specifications

Appendix B

Measurement graphs

B.1 Accelerometer linearity measurement graphs

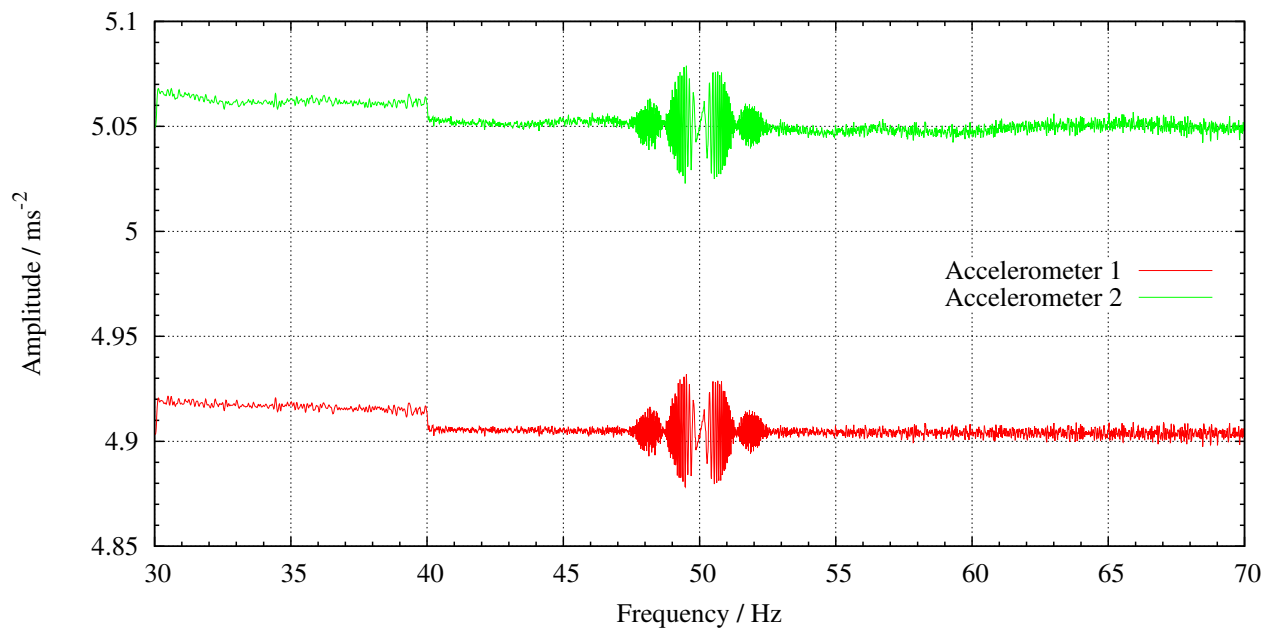


Figure B.1.1: 50 Hz measurement graphs.

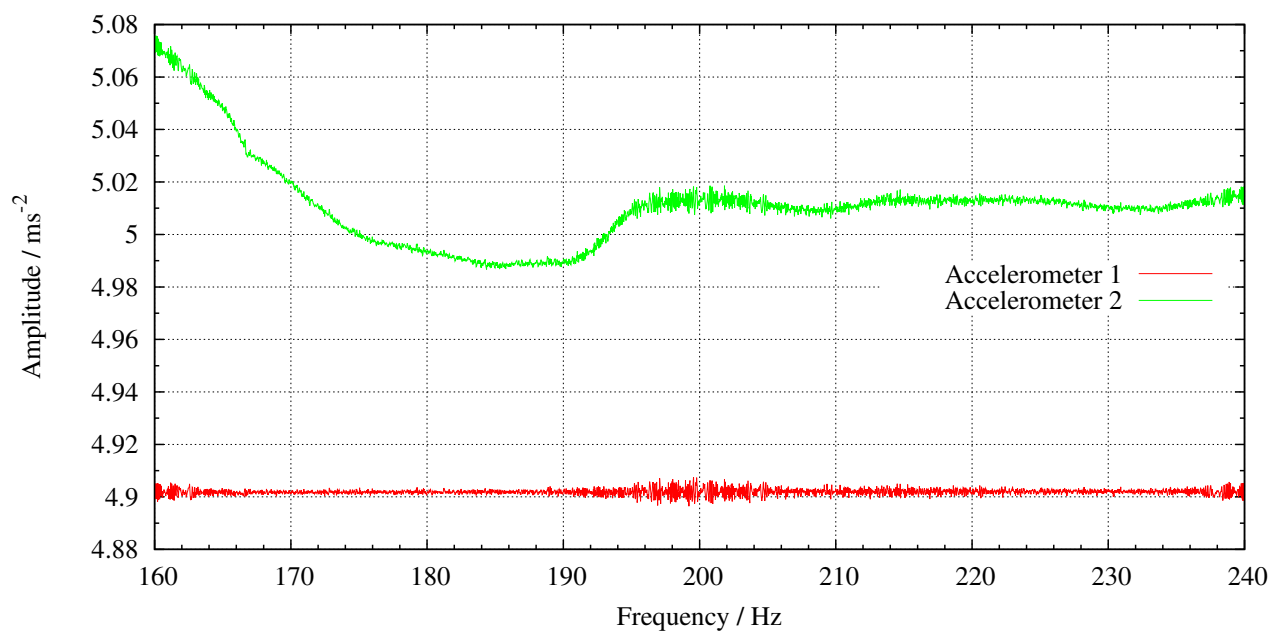


Figure B.1.2: 200 Hz measurement graphs.

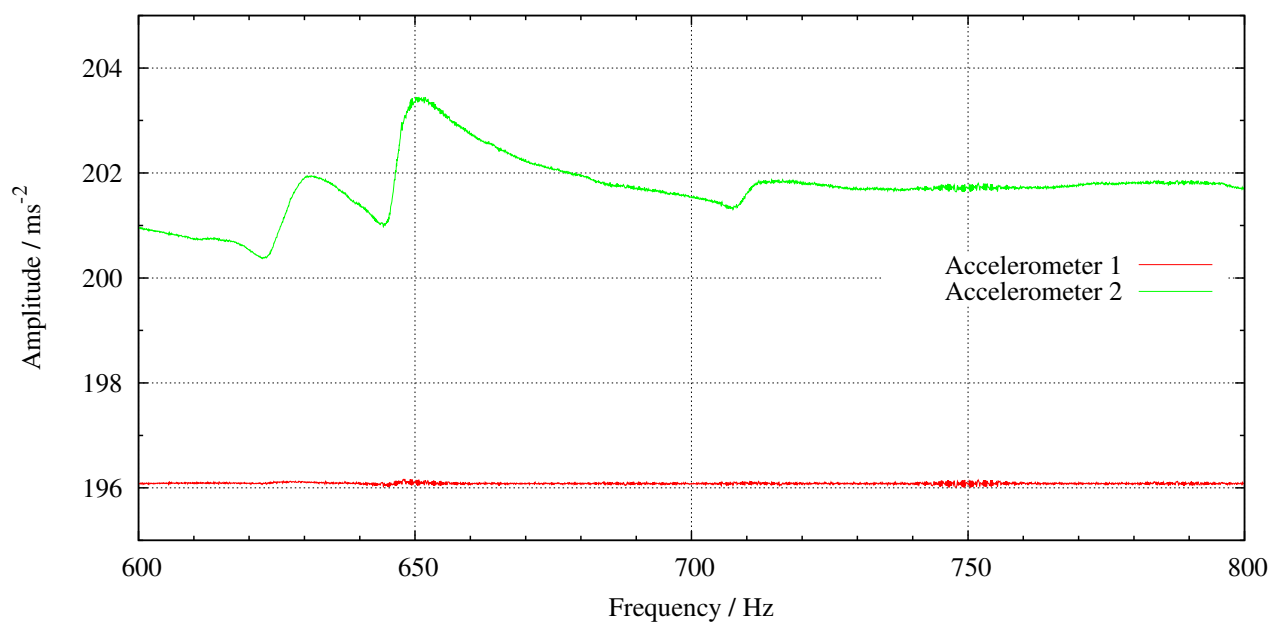


Figure B.1.3: 700 Hz measurement graphs.

B.2 Repeatability measurement graphs

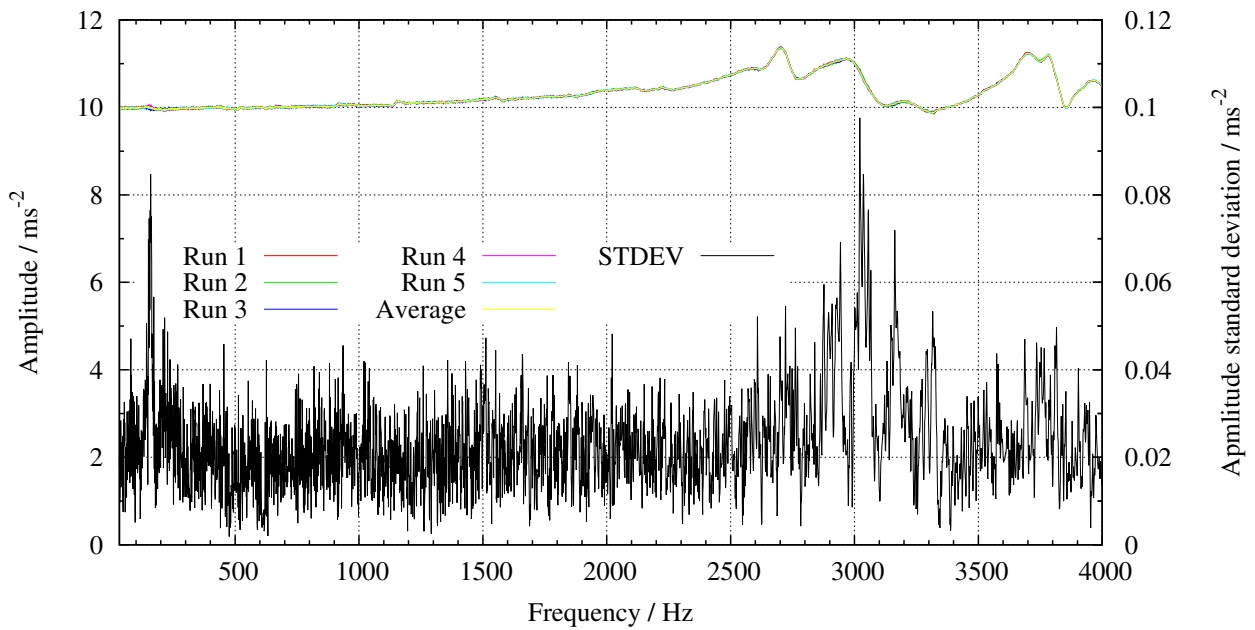


Figure B.2.1: Graphs of first repeatability measurement set results.

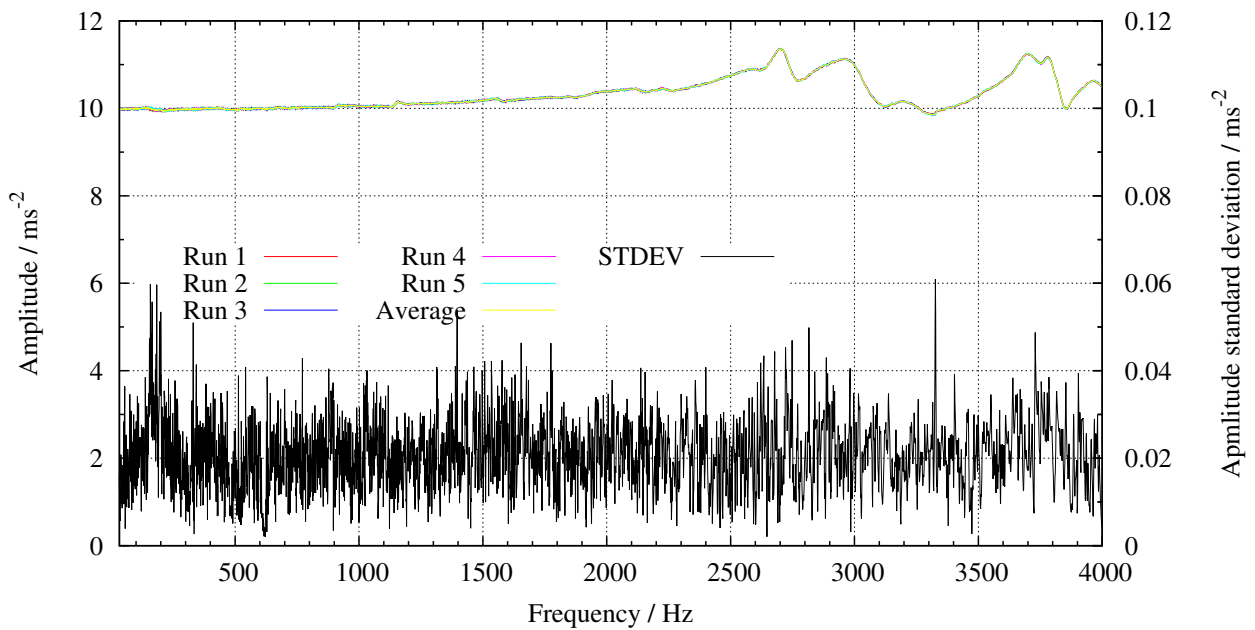


Figure B.2.2: Graphs of second repeatability measurement set results.

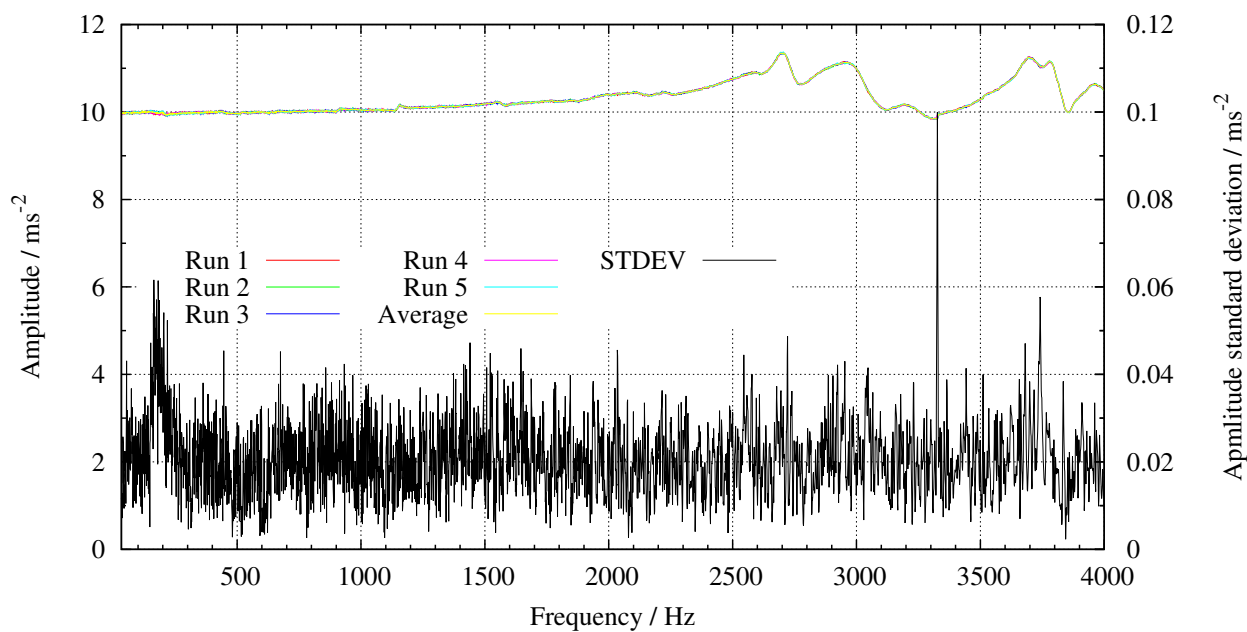


Figure B.2.3: Graphs of third repeatability measurement set results.

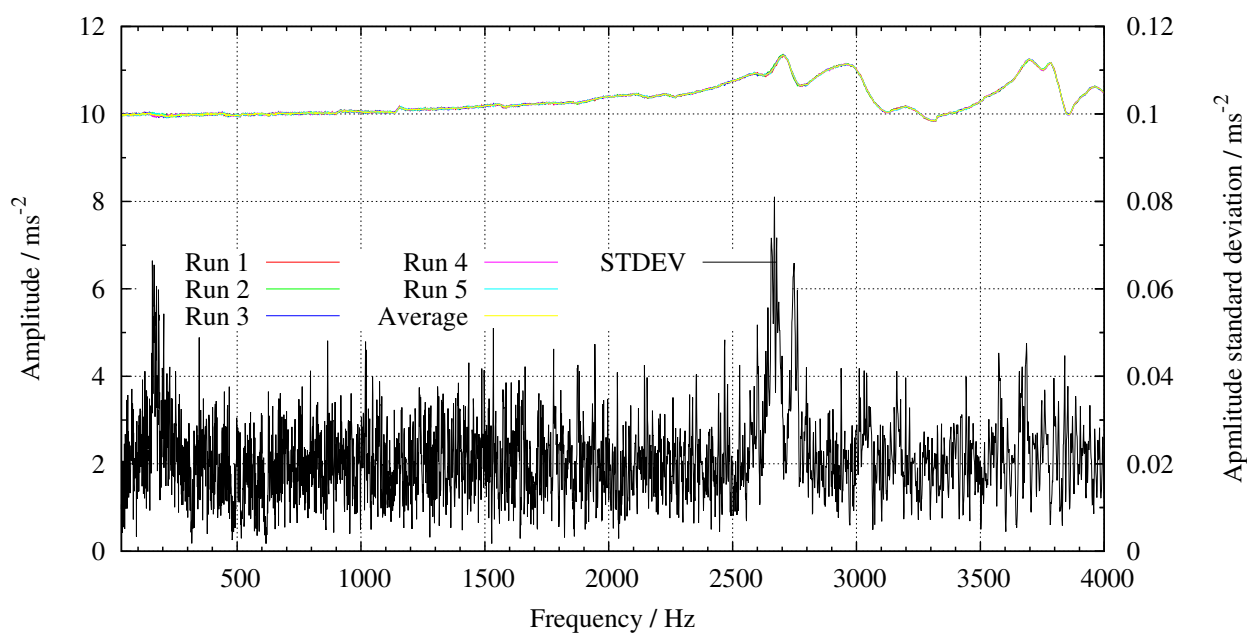


Figure B.2.4: Graphs of fourth repeatability measurement set results.

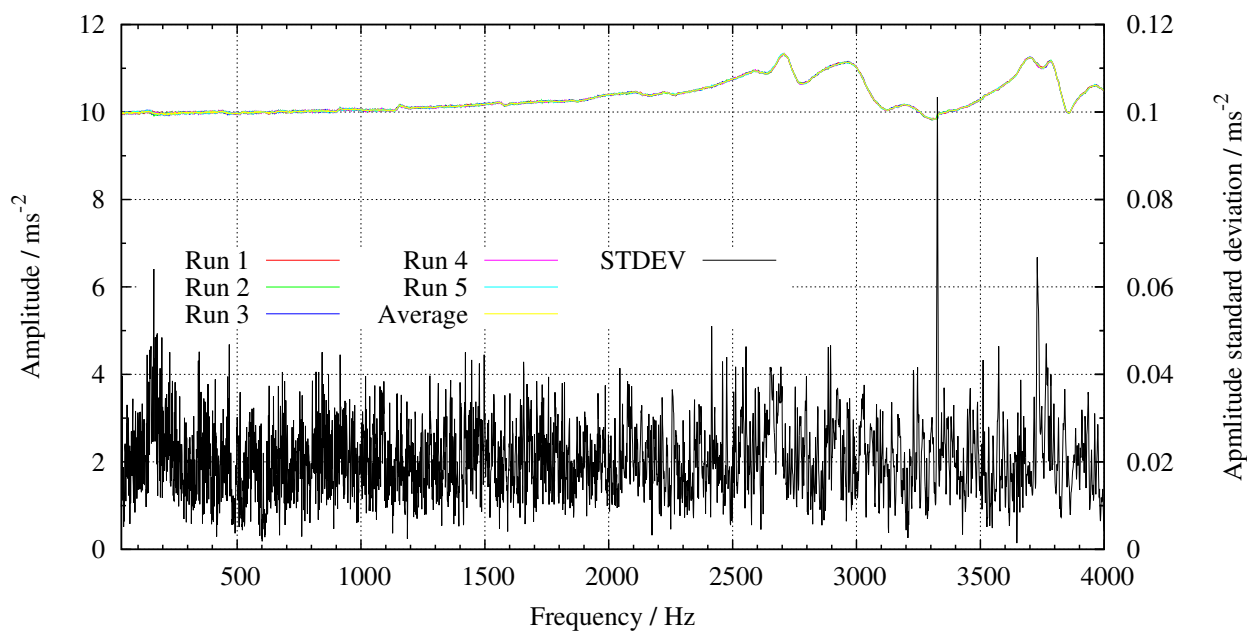


Figure B.2.5: Graphs of fifth repeatability measurement set results.

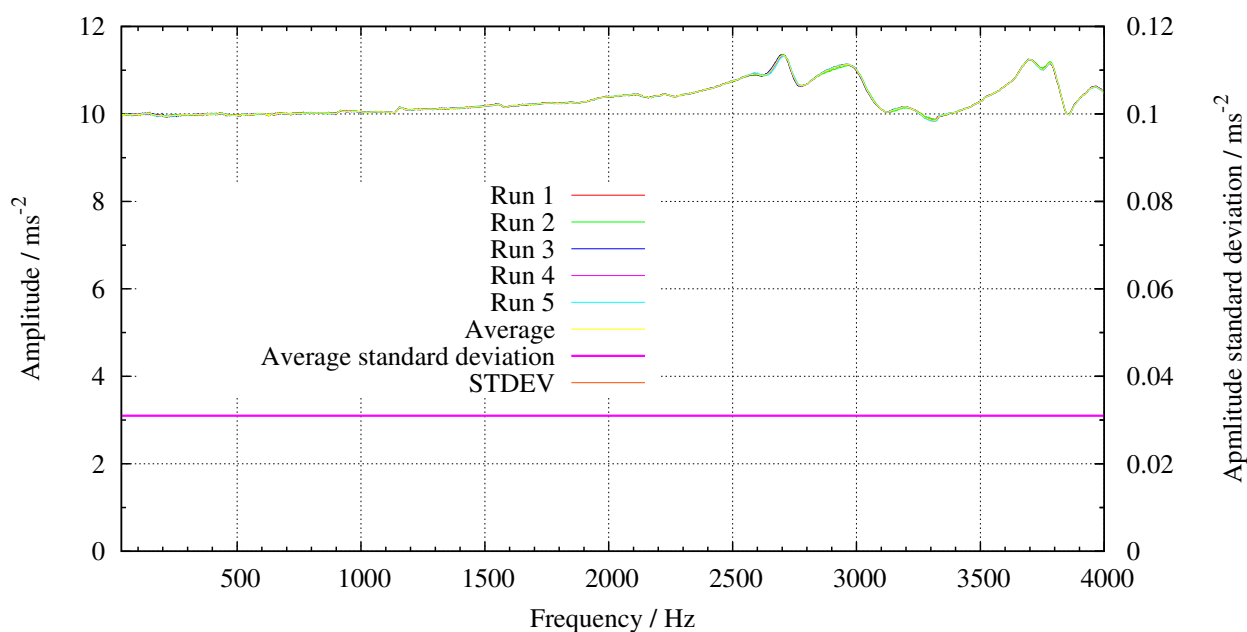


Figure B.2.6: Graphs of pooled repeatability measurement set results.

B.3 Frequency validation measurement graphs

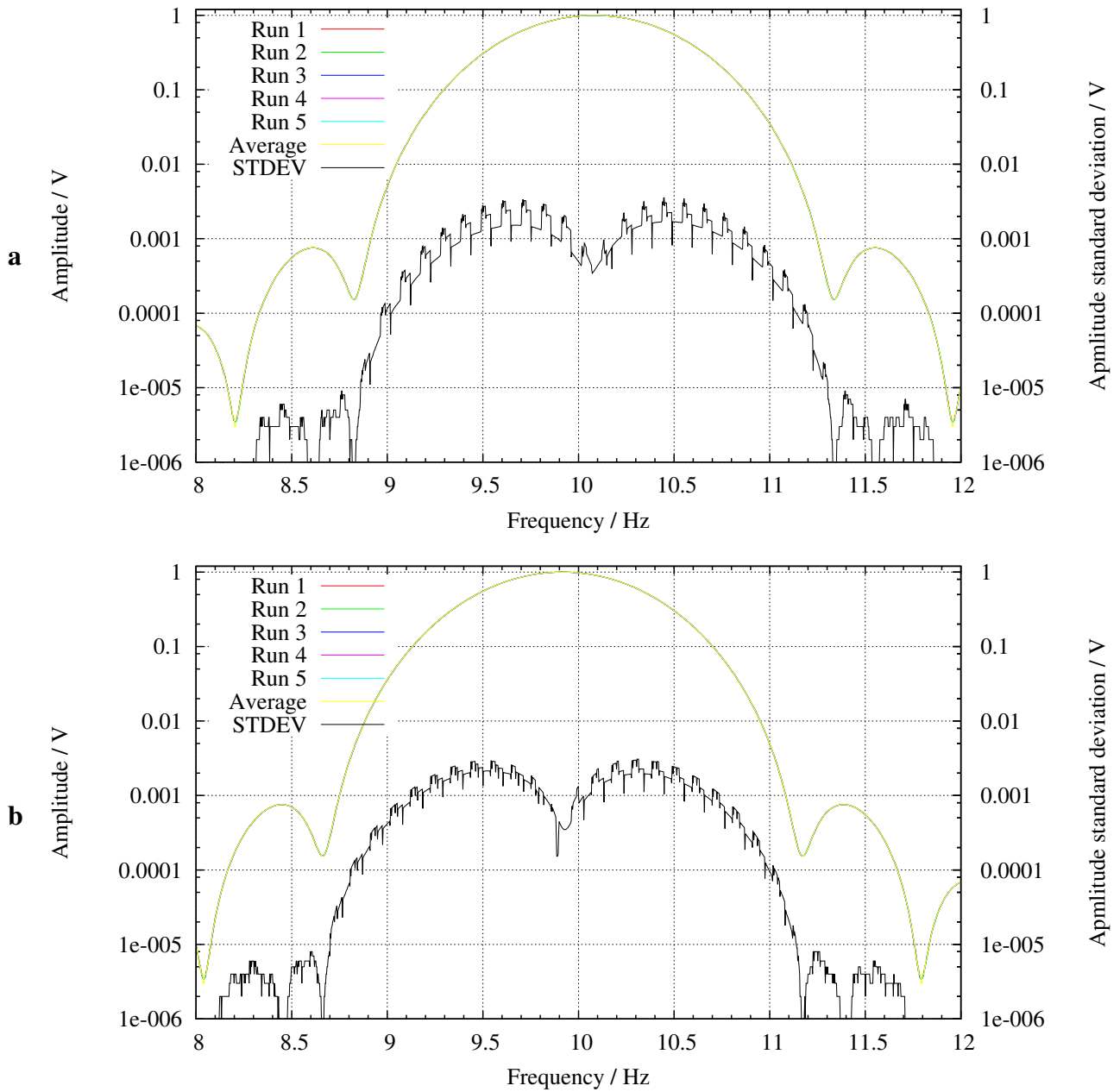


Figure B.3.1: 10 Hz frequency verification graphs. a) “up” sweeping direction; b) “down” sweeping direction.

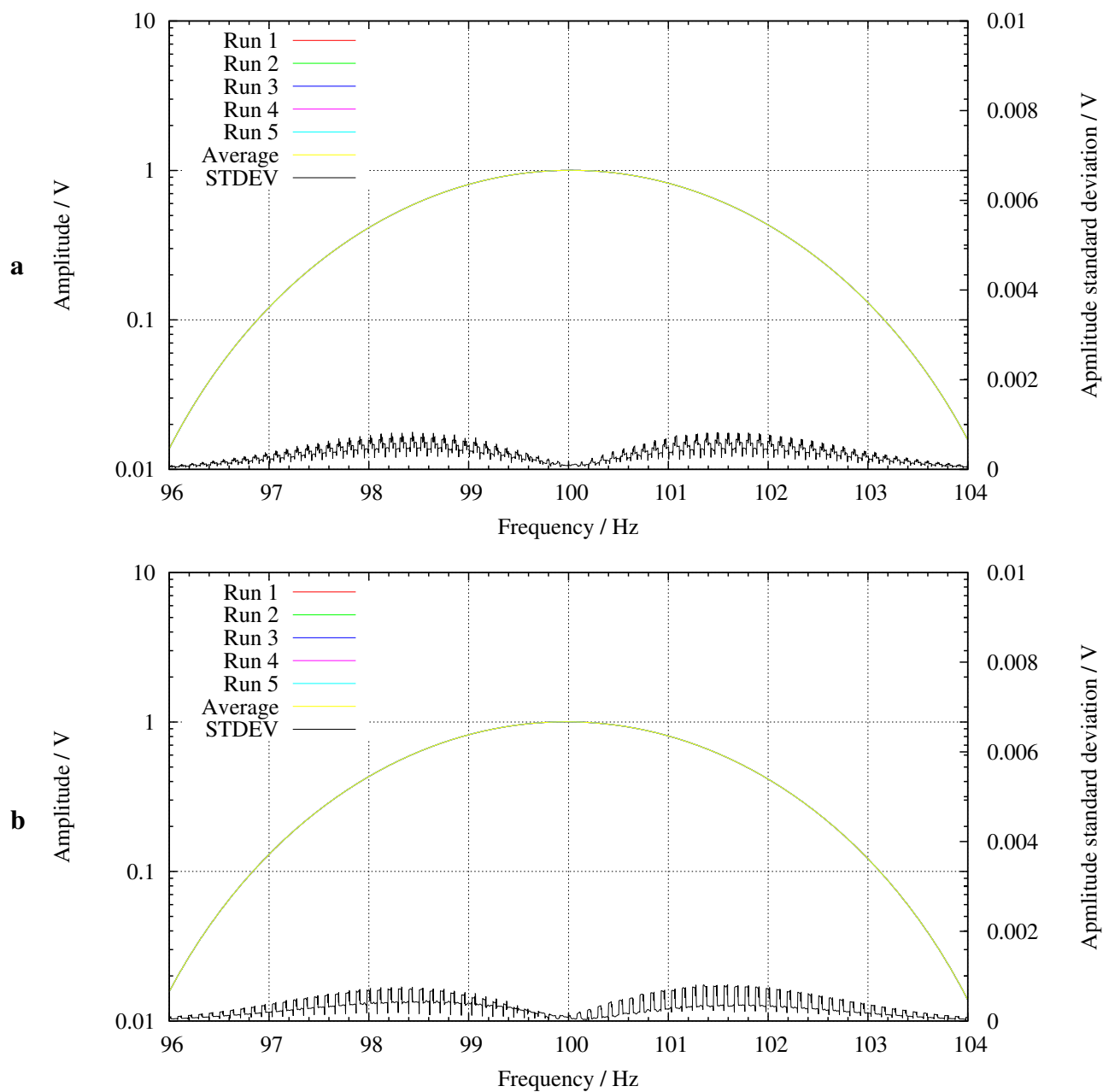


Figure B.3.2: 100 Hz frequency verification graphs. a) “up” sweeping direction; b) “down” sweeping direction.

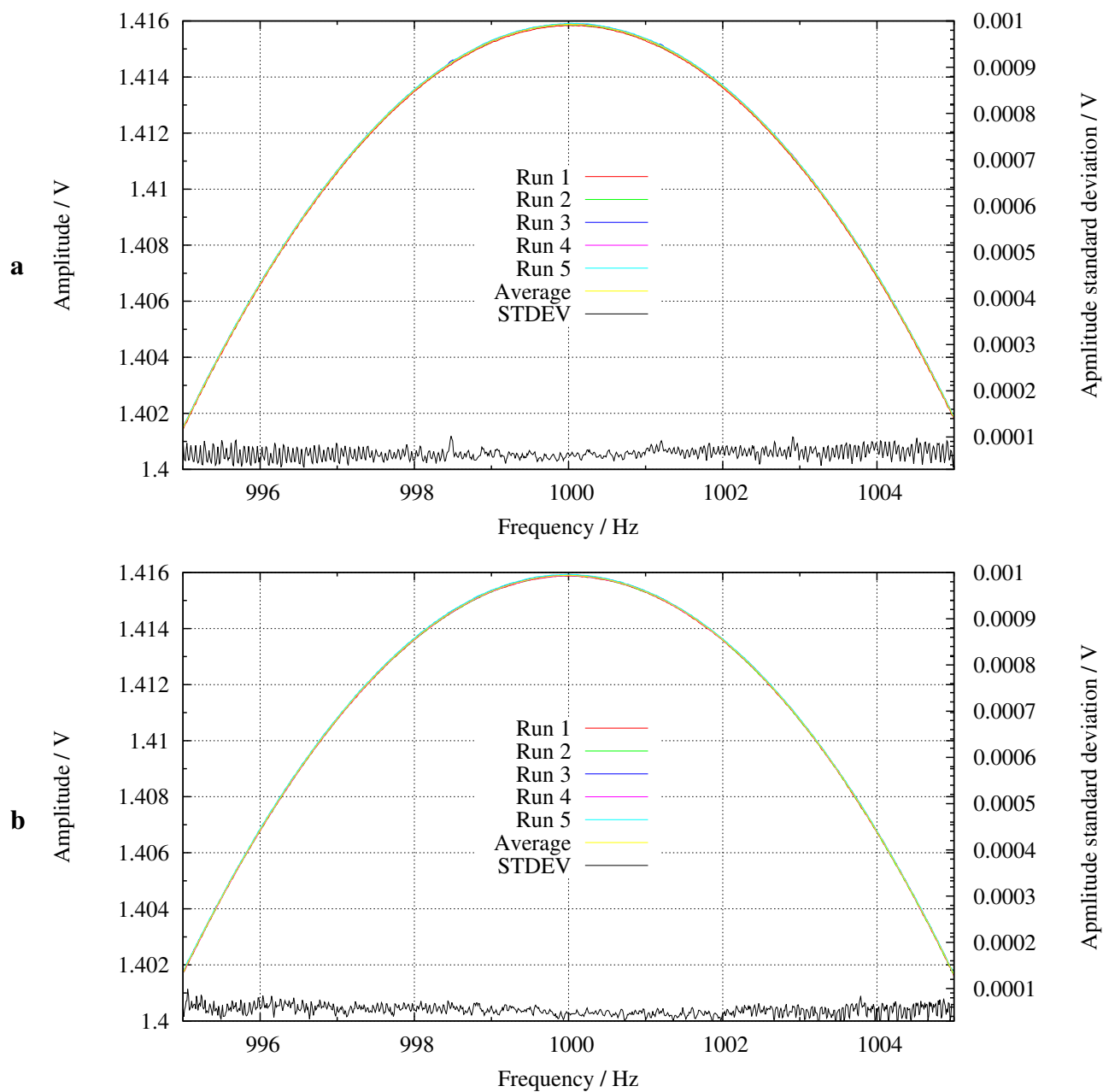


Figure B.3.3: 1 kHz frequency verification graphs. a) “up” sweeping direction; b) “down” sweeping direction.

Appendix C

Program code of scripts used

C.1 Repeatability calculation and graph generation scripts

Python™ script code in Listing C.1 is used for calculating repeatability parameters from input CSV files, output graphs are generated by Gnuplot script in Listing C.2.

```
import re
import os
import math

lines_to_skip = 28
workingdir = os.path.dirname(os.path.realpath(__file__))

##### Constants for corrections and uncertainties
# graviational constant
G = 9.80665
# accelerometer sensitivity mV/g
accSens = 9.743
### Constants for thermal correction calculation
# starting time in minutes from turning on the bench
startTime = 120
# test duration in seconds. Typical values for 2 oct/min = 270 sec ,
# 1 oct/min = 547 sec
testDuration = 270
# choose which logfit to use. THESE CONSTANTS HAVE TO BE UPDATED
# ACCORDINGLY!
if startTime < 200:
    def y(x) :
        return math.log(x) * 3.9017 + 7.1145
else:
    def y(x) :
```

```

        return math.log(x) * 1.3336 + 20.089
# read number of samples
num_lines = sum(1 for line in open('run_(1).csv'))-lines_to_skip
timeFraction = float(testDuration) / float(num_lines)
#### End of thermal constants

# gain error of controller / %
gainErr = 0.000000
# controller input offset / V (assmed gradual change)
def contrOffset(f):
    if 0 <= f < 100:
        return f/(100-0) * (0.0000000-0.0005705)
    if 100 <= f < 1000:
        return f/(1000-100) * (0.0005705-0.0000097)
    else:
        return 0.0000097

### uncertainty sources
# DSP float error / V
uDSP = 0.00000034
# ADC quantization error / V
uADC = 0.0000576687
# CMRR noise / V
uCMRR = 0.00000006
# transverse sensitivity / ms**-2 * G
uTrans = 0.049/G
# reference sensitivity / ms**-2 * G
uRef = 0.005/G
# temperature uncertainty / ms**-2/'C * G
uTemp = 0.008/G
# Reproducibility / ms**-2 * G
uRep = 0.0324/G
# definition of Gaussian curve
def gaussian(x, mu, sig):
    return math.exp(-pow(x - mu, 2) / (2 * pow(sig, 2)))
# linearity offsets from stated slope
def uLin(f):
    if 5.5 <= f < 6.5:
        return 0.04 * gaussian(6, f, 0.1)
    if 7 <= f < 13:
        return 0.02 * gaussian(10, f, 1)

```

```

    if 42 <= f < 52:
        return 0.02 * gaussian(6, f, 0.1)
    if 160 <= f < 240:
        return 0.01 * gaussian(45, f, 2)
    if 650 <= f < 750:
        return 0.005 * gaussian(700, f, 10)
    else:
        return 0
# inherent noise / ms**-2
uInh = 0.008
# DMM amplitude total uncertainty
def uDMA(f):
    # 500 Hz was coefficient change
    if 0 <= f < 500:
        return 0.0366
    else:
        return 0.0372

##### End of Constants for corrections and uncertainties

print ("Working_in_%s" %workingdir)
os.chdir(workingdir)
# open files
with open('run_(1).csv', 'r') as run1, open('run_(2).csv', 'r') as
    run2, open('run_(3).csv', 'r') as run3, open('run_(4).csv', 'r')
        as run4, open('run_(5).csv', 'r') as run5, open('out.csv', 'w')
            as fout:
    # read files into lists with skipping headers
    lines1 = run1.readlines()[lines_to_skip:]
    lines2 = run2.readlines()[lines_to_skip:]
    lines3 = run3.readlines()[lines_to_skip:]
    lines4 = run4.readlines()[lines_to_skip:]
    lines5 = run5.readlines()[lines_to_skip:]
    # iterate over all list elements
    for index, item in enumerate (lines1):
        # fill temporary lists with current line
        templine1 = lines1[index]
        templine2 = lines2[index]
        templine3 = lines3[index]
        templine4 = lines4[index]

```



```

templene5 = lines5[index]
# read out frequency
f=float(templene1.split(',')[0])
# calculate amplitude mean value
meanA=(float(templene1.split(',')[1])+float(
    templene2.split(',')[1])+float(templene3.split(
    ','),')[1])\
    +float(templene4.split(',')[1])+float(
    templene5.split(',')[1]))/5
# calculate sensitivity change at this frequency
sensCorr = math.log10(f/159.2)*0.026*meanA
# calculate temperature offset
tempCorr = (y(int(timeFraction*index/60)+int(
    startTime))-25)*0.0009*meanA
# calculate gain correction to be applied
gainCorr = meanA * gainErr
# apply all the correction factors to measured mean
meanCorr = meanA + sensCorr + tempCorr - gainCorr +
    contrOffset(f)
# calculate amplitude standard deviation
stdevA= (pow((pow((float(templene1.split(',')[1])-
    meanA),2)+pow((float(templene2.split(',')[1])-
    meanA),2)\
    +pow((float(templene3.split(',')[1])-meanA
    ),2)+pow((float(templene4.split(',')[1])-meanA
    [1])-meanA),2)\
    +pow((float(templene5.split(',')[1])-meanA
    ),2)),0.5))
# total uncertainty
uTotal = pow(pow(stdevA,2) + pow(uLin(f)*meanA,2)+
    pow(uDMMA(f)*meanA,2)+pow(uInh,2)+\
    pow(uTemp*(y(int(timeFraction*index/60)+
    int(startTime))-25),2)+pow(uRef,2)+pow(
    uRep,2)+\
    pow(uDSP*accSens,2)+pow(uADC*accSens,2)+
    pow(uCMRR*accSens,2)+pow(uTrans,2),0.5)
# write out calculated values into output file
fout.write('%f,%f,%f,%f,\n' %(f, meanA, uTotal,
    meanCorr))
# close files

```

```
run1.close()  
run2.close()  
run3.close()  
run4.close()  
run5.close()  
fout.close()  
print ('Done')
```

Listing C.1: Python code for repeatability parameter calculations

```

set datafile separator ","
set terminal postscript eps size 6,3 enhanced color solid font '
    Times–roman,18'
set output 'corr_w_unc.eps'
set xlabel "Frequency_/_Hz"
set ylabel "Amplitude_/_ms^{−2}"
set y2label "Relative_/_uncertainty_/_%"
set y2tics
set xtics
set mxtics
set mytics
set my2tics
set grid xtics mxtics ytics
set key top left
set yrange [5:15]
set xrange [35:4000]
set y2range [0:10]
show grid
#set log x
set style fill solid
plot "out.csv" using 1:($4*9.80665):(($4*9.80665−$3*9.80665)) with
    filledcurves above ti "Uncertainty_region" linecolor rgb "#
    FF0000",\
"out.csv" using 1:($4*9.80665):(($4*9.80665+$3*9.80665)) with
    filledcurves below notitle linecolor rgb "#FF0000",\
"out.csv" using 1:($4*9.80665) with lines linecolor rgb "#000000"
    ti "Corrected_average",\
"out.csv" using 1:($2*9.80665) with lines ti "Uncorrected_average"
    linecolor rgb "#00FF00",\
"out.csv" using 1:((($3/$4)*100) with lines ti "Relative_/_uncertainty
    " axis xly2
quit

```

Listing C.2: Gnuplot script for generating repeatability graphs with standard deviations

Non-exclusive license to reproduce thesis and make thesis public

I, Kaspars Laizans, (date of birth: 06.08.1986.),

1. herewith grant the University of Tartu a free permit (non-exclusive license) to:

1.1 reproduce, for the purpose of preservation and making available to the public, including for addition to the DSpace digital archives until expiry of the term of validity of the copyright, and

1.2 make available to the public via the university's web environment, including via the DSpace digital archives, as of 09.06.2014 until expiry of the term of validity of the copyright,

“A method for characterization of vibration testing setups”

(title of thesis)

supervised by PhD Riho Vendt

2. I am aware of the fact that the author retains these rights.

3. This is to certify that granting the non-exclusive license does not infringe the intellectual property rights or rights arising from the Personal Data Protection Act.

Tartu 27.05.2014